RATCHETING BEHAVIOUR OF AISI 316L STAINLESS STEEL

A THESIS WORK SUBMITTED IN PARTIAL FULFILMENT REQUIREMENT FOR THE AWARD OF THE DEGREE OF

Master of Technology in Material Engineering

Faculty of Engineering and Technology

Department of Metallurgical and Material Engineering

JADAVPUR UNIVERSITY

SESSION: 2020-2022

By

Sonal Kumar singh

Registration. No. 154365 of 2020-2021

Examination Roll No. M4MAT22003

UNDER THE GUIDANCE

of

Prof. Pravash Chandra Chakraborti

Department of Metallurgical and Material Engineering

Faculty of Engineering and Technology

Jadavpur University

Kolkata: 700032

FACULTY OF ENGINEERING & TECHNOLOGY

METALLURGICAL AND MATERIAL ENGINEEERING DEPARTMENT

JADAVPUR UNIVERSITY

CERTIFICATE OF APPROVAL

This is to certify that I have examined the thesis entitled "**Ratcheting behaviour of AISI 316L stainless steel**" submitted by Sonal Kumar Singh and here by accord my approval of it as a study carried out and presented in a manner required for its acceptance in the field of Metallurgical and Material Engineering.

Committee of
Final Examination for
Evaluation of the thesis

FACULTY OF ENGINEERING & TECHNOLOGY

METALLURGICAL AND MATERIAL ENGINEEERING DEPARTMENT

JADAVPUR UNIVERSITY

RECOMMENDATION CERTIFICATE

This is to certify that we have examined the thesis entitled "**Ratcheting behaviour of AISI 316L stainless steel**" submitted by Sonal Kumar Singh and accepted in partial fulfillment of the requirement for the degree of Master of Technology in Material Engineering. It is bonafide work carried out by him under our guidance.

Prof. Pravash Chandra Chakraborti
Head of the Department
Department of Metallurgical and Material Engineering
Jadavpur University, Kolkata-700032

Prof. Chandan Mazumdar
Dean - Faculty of Engineering and Technology (FET)
Jadavpur University, Kolkata-700032

Prof. Pravash Chandra Chakraborti
Thesis Supervisor
Department of Metallurgical and Material Engineering
Jadavpur University, Kolkata-700032

FACULTY OF ENGINEERING & TECHNOLOGY

METALLURGICAL AND MATERIAL ENGINEEERING DEPARTMENT

JADAVPUR UNIVERSITY

DECLARATION

I do hereby solemnly declare that the research work embodied in this thesis "**Ratcheting Behaviour of AISI 316L stainless steel**" is the original investigation carried out by me under the supervision of **Prof. Pravash Chandra Chakraborti**, Dept. of Metallurgical & Materials Engineering, Jadavpur University, Kolkata, India for the award of the degree of Master of Technology in Material Engineering of Jadavpur University. To the best of my knowledge and belief, this work has not been presented for any degree or distinction under any other university.

Sonal Kumar Singh
Department of Metallurgical & Material Engineering
Jadavpur University

Date:
Place: Kolkata

ACKNOWLEDGEMENT

I would like to express my gratitude and appreciation to all those who gave me the possibility to complete this thesis.

Special thanks is due to my supervisor **Prof. Pravash Chandra Chakraborti**, Department of Metallurgical & Materials Engineering, Jadavpur University, whose help, stimulating suggestions and encouragement helped me in all time of fabrication process and in writing this report.

I am also thankful to the librarian and technical staffs of Metallurgical and Material Engineering Department, Jadavpur University for their cordial assistance.

My special gratitude to **Mr. Shantanu Jana** for his all time assistance and guidance from the very beginning of this project.

Special thanks to **Mr. Manish Kumar Patel**, **Mr. Chandesham Prabhakar** and **Mr. Rahul Kumar** for their support and encouragement during this research work. I thankfully acknowledge the support of all those people, who some time or the other directly or indirectly rendered their help at different stages of this work.

I am very much thankful to my friends and classmates, specially **Mr. Pratik Raj**, **Mr. Suraj kumar** and **Mr. Vivek Kumar** for their useful assistance and support. Last but not the least, special thanks to my beloved parents, as they always stood by me, caring least the prevalent situation.

CONTENTS

List of Tables

List of Figures

ABSTRACT

Austenitic stainless steels are the most widely used variant of stainless steel. They contain very low levels of carbon and high amounts of nickel and chromium, which are the main contributors to their formability, corrosion-resistance and wear-resistance. They are also non-magnetic in their annealed state but can become slightly magnetic when cold worked. Microstructural analysis of the steel must be understood with respect to its specific applications. Knowledge of fracture mechanisms, nucleation, micro and macro-crack propagation under low cycle fatigue conditions are crucial especially for high-risk systems such as nuclear applications . Due to the highly customisable nature of austenitic stainless steels, it has been used for a wide range of applications, from the medical sector to the automobile industry.

The aim of this report is to examine the nature of strain accumulation in ratcheting of AISI 316L stainless steel. Stress-controlled ratcheting test has been carried out at a constant stress rate of 200MPa/s while mean stress and amplitude stress are varied and maximum stress is kept constant.

In the present investigation an attempt has been made to study the effect of various stress parameters on ratcheting behaviour of 316L stainless steel. In this investigation the different combinations of mean stress and amplitude stress are taken while keeping the maximum stress constant, the experiments are conducted on 316L specimen.

To understand the ratcheting behaviour of steel various approaches such as (i) ratcheting strain % (ii) Ratcheting strain rate (iii) strain energy density, (iv) cyclic stress-strain curve and (v) Strain energy density vs mean stress are utilized in this investigation.

The investigation results have been finally analyzed by the use of graph which are plotted to find out the effect of different parameters on ratcheting. Fractographic analysis has also been carried to visualize the detrimental effect of ratcheting on 316L stainless steel more clearly.

CHAPTER-1

INTRODUCTION

1.1 BACKGROUND AND MOTIVATION

Steel is an alloy of iron and carbon and other elements. Steel is the most important alloy which is used as a structural material. Steel is an alloy formed by combining iron and small amount of carbon content (0.2% and 2.1% by weight) depending upon the type. Lakhtin Y. in his book [1] explained that carbon is the most appropriate material for iron to make bond in steel; it also solidifies the inherent structures of iron.

Austenitic stainless steels are important engineering materials, readily employed in high temperature applications such as in nuclear reactors due to their excellent mechanical properties, corrosion resistance and weldability [2]. Metastable austenitic stainless steels show complex changes in their microstructure during deformation and hence changes in the mechanical performances of the materials. This is primarily due to the evolution of martensite on deformation [3]. A number of parameters play a major role in the deformation induced martensitic transformation and the mechanical behaviour of these alloys. Austenitic steels have better strength-elongation combination as compared to other structural alloys and therefore they have found extensive application for critical components like heat transport piping of nuclear power plants [2].

1.2 OBJECTIVE

This thesis is focused on tensile behaviour and ratcheting behaviour of the austenitic stainless steel 316L grade. The objective of the present investigation is to observe the effect of various stress parameters on ratcheting behaviour of stainless steel at different combinations of mean stress and stress amplitude while keeping the maximum stress constant. The complete test is carried out at a stress rate of 200MPa/s.

CHAPTER-2

LITERATURE REVIEW

2.1 INTRODUCTION

"Stainless" steel is actually a generic term referring to a variety of steel types. Like all other kinds of steel, stainless steel is made primarily from iron and carbon in a two-step process. What makes stainless steel different is: the addition of chromium (Cr) and other alloying elements such as nickel (Ni) to create a corrosion-resistant product.

Steel corrodes because iron, the metal used to make steel, occurs in nature in combination with other elements. When iron ore is artificially manipulated into a pure form to make steel, it becomes unstable and will readily recombine with oxygen.

When chromium is added to steel, it forms chromium oxide, which acts as a protective surface to prevent air and moisture from causing rust, as happens with ordinary steel. Chromium is added in quantities ranging from 10.5 to 30%, depending on the application or environment in which the steel is to be used [4]. There are more than 100 different grades of stainless steel but they are often classified in five different types, named after their structure:

a) **Ferritic stainless steel**

It has similar properties to mild steel (the most common steel), but better corrosion, heat, and cracking resistance. Ferritic steel is commonly used in washing machines, boilers and indoor architecture [54].

b) **Martensitic stainless steel**

It is very hard and strong, though it is not as resistant to corrosion as austenitic or ferritic grades. It contains approximately 13% chromium and is used to make knives and turbine blades [54].

c) **Austenitic Stainless steel**

It is the most widely used type of stainless steel. It has excellent corrosion and heat resistance with good mechanical properties over a wide range of temperatures. Austenitic steel is used in housewares, industrial piping and vessels, construction, and architectural facades [54].

d) **Duplex stainless steel**

It is a composite of austenitic and ferritic steels, making it both strong and flexible. Duplex steels are used in the paper, pulp, shipbuilding, and petrochemical industries. Newer duplex grades are being developed for a broader range of applications [54].

e) **Precipitation hardened steel**

Martensitic or semi-austenitic steels can also be classified as **precipitation hardening** stainless steels. These steels are made to be extremely strong with the addition of elements such as aluminum, copper and niobium. Corrosion resistance is the main advantage of stainless steel, but it certainly isn't the only one. Stainless steel is also [54]:

- High and low temperature resistant
- Easily fabricated
- Strong and durable
- Easy cleaned and maintained
- Long lasting, with a low lifecycle cost
- Aesthetically attractive
- Environmentally friendly and recyclable.

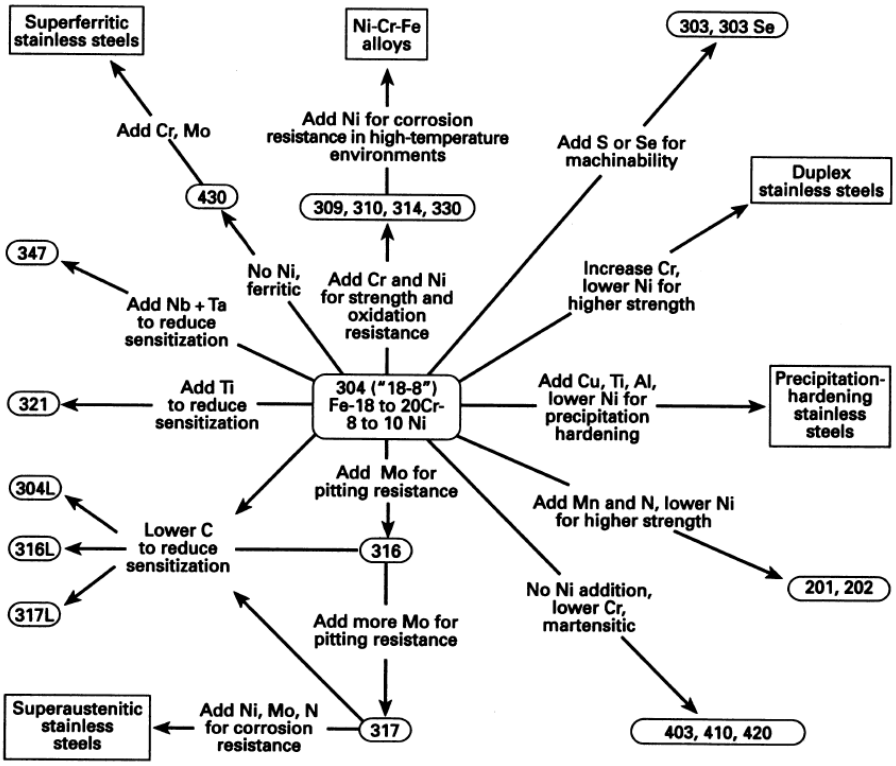

Fig. 2.1: *Composition and property linkages in the stainless steel family of alloys [45]*

Ferrite is the basic crystal structure of iron or low-alloy steel at ambient temperatures having BCC crystal structure. Austenite is the crystal form of unalloyed iron in the grains at higher temperature (>800°C). As in ferrite, there is an atom at each corner of a cube, but instead of one in

the geometric centre, there is one in the centre of each of the six faces of the cube. This face-centred cubic array becomes stable at room temperature if nickel, manganese, nitrogen, or carbon is added, singly or in combination, to iron or iron/chromium alloys. The resulting materials are called austenitic stainless steels. In general, they are easier to shape and bend, more weldable, and less brittle than ferritic alloys.

They are always iron-chromium alloys, but they often contain other elements, such as molybdenum or nickel. Nickel in stainless steel promotes austenite stability and reduces the temperature at which austenite can exist. Manganese is similar to nickel when it is added to or substituted for nickel and also increases strength. Molybdenum increases the resistance to localized corrosion phenomena, such as pitting and crevice corrosion.

2.2 PHASE BALANCE IN STAINLESS STEEL

In a metal, groups of crystals having the same crystal structure are called phases. The phase names for the three crystal structures present in stainless steels are austenite, ferrite, and martensite. The metallurgist uses a technique of polishing and etching the surface of a small sample to identify and quantify the phases present. The metallurgist uses chemical composition and heat treatment to control the quantity and type of phases present in the steel. Ferrite-forming elements foster formation of ferrite, while austenite-forming elements promote the formation of austenite.

Table 2.1: Some ferrite formers and austenite formers in Stainless Steel [5]

Ferrite Formers	Austenite Formers
Iron	Nickel
Chromium	Nitrogen
Molybdenum	Carbon
Silicon	Manganese
Niobium	Copper
Aluminium	Cobalt
Titanium	
Tungsten	

Table2.1 lists the common ferrite and austenite forming elements. The “phase balance” (relative amounts of different phases) of a steel determines its properties. Controlling the steel’s phase balance, and therefore its properties, demands a balance of the alloying elements. The Schaeffler Diagram (Figure2.2) is a tool that shows the relationship between the chemical composition and the phases present in stainless steels. In the as-cast condition, as might be found in a weld. It allows the user to determine the phase balance from a given specified composition. The diagram shows that minor variations in carbon or silicon content can have a great effect on the phase balance [5].

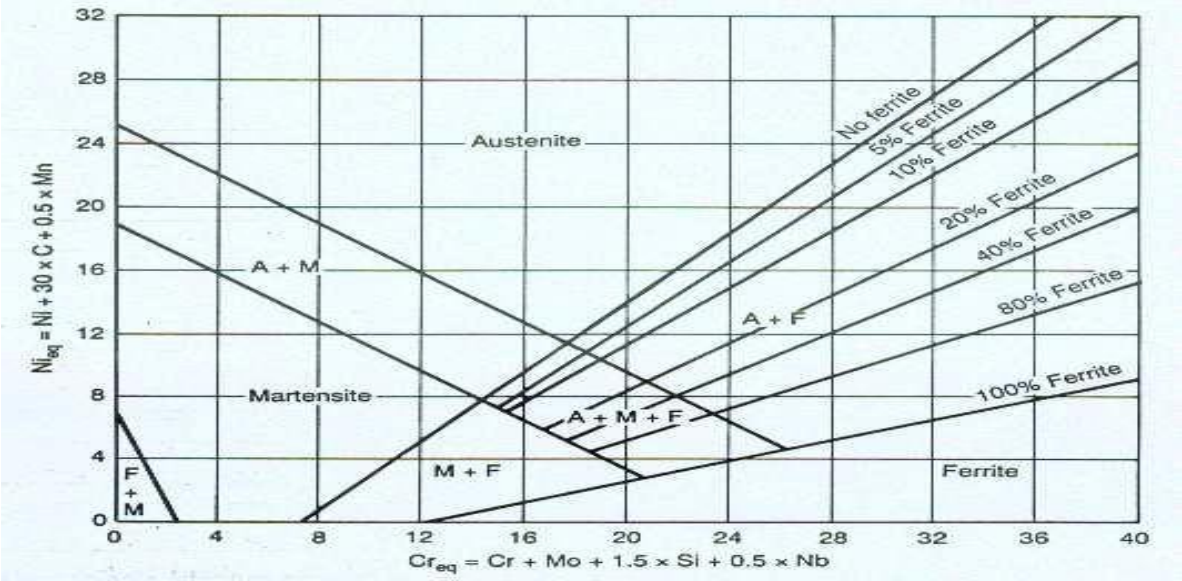

Fig 2.2: *The Schaeffler Diagram shows the influence of chemical composition on the amount of ferrite and austenite in the microstructure of as-cast weld metal [5].*

2.3 AUSTENITIC STAINLESS STEEL

The term austenite is used to describe a face-centered cubic (FCC) iron or steel alloys that have this type of structure. It was named after Sir William Chandler Roberts-Austen, an Englishman known for his studies of the physical properties of metals.

This is the most commonly used type of stainless steel, and with good reason. With its exceptional resistance to heat and corrosion, it's used extensively in many industries including medical, automotive, aerospace, and industrial applications. This category is known for unsurpassed strength and formability and that it cannot be hardened by heat treatment.

Austenitic stainless steels are alloyed with nickel so as to allow for the retention of the high temperature face centered cubic (FCC) austenite (γ) phase to room temperature [54].

Steel becomes 'austenite' by nature when nickel or nitrogen is added to it. It is the chemical composition that dictates the exact grade of stainless steel, while the austenite crystalline structure in the material itself is a central characteristic [54].

In the annealed condition it is important to note that Austenitic stainless steel is usually characterized as non-magnetic, however cold rolling austenitic steel, or reducing its thickness and increasing its hardness, introduces a certain amount of magnetism to the material.

Austenitic stainless steel is highly regarded for its formability, making it well suited for fabrication. Its resistance to corrosion also makes it a popular choice where this is a consideration within an application [54].

Chemical Composition

Austenitic stainless steel comprises a minimum of 10.5% chromium and 8 to 12% nickel, as well as nitrogen and a range of other elements in solution. It is chromium that gives the steel its considerable corrosion resistance, while nitrogen acts as a stiffening agent [54].

Austenite Crystalline Structure

Stainless steel that presents an austenite crystalline structure, as well as the face-centered-cubic lattice structure, remains present throughout both hot and cold temperatures. Magnesium, nickel, and nitrogen are the stabilizing elements of the austenite structure [54].

Characteristics of Austenitic stainless steel

Austenitic stainless steel has a number of beneficial attributes which make it a material that is highly in demand. These attributes include:

Strength at Temperature

Austenitic stainless steel can endure extreme temperatures. Depending upon the grade, these can be up to around 1900 °F. Some grades, however, do start to exhibit softening, deforming or loss of strength at 800 °F [54].

Cold Workability

As mentioned previously, austenitic stainless steels can't be hardened using heat treatment and only cold working or reduction are able to enhance the strength of austenitic. Cold working in this context refers to shaping metal without heating it [54].

Additionally, austenitic stainless steels can be annealed before quickly cooling or 'quenching' the metal to return it to its initial state. Cold rolled stainless steel offers a range of benefits including, most notably, enhanced surface finish. This is a useful trait, as steel with an improved surface finish will possess higher hardness, making it stronger and more resistant to crack propagation [54].

Low Thermal Conductivity

Heat does not travel quickly through austenitic stainless steel. On the other hand, ferritic stainless steel possesses a higher thermal conductivity [54].

Formability

Austenitic stainless steel is extremely formable, meaning it is a versatile material that is suitable for an array of applications.

While cold working austenitic stainless steel increases its strength, it also decreases its ductility. Austenitic stainless steel possesses a higher susceptibility to stress corrosion cracking than ferritic [54]. Austenitic stainless steel is typically not magnetic, while ferritic stainless steel is generally magnetic. Where, for example, some refrigerators are magnetic while others are not, this is simply because they are made of differing types of stainless steel.

There are exceptions to the above, however, and specific processes or temperatures can cause the stainless steels crystal structure to rearrange, giving the material magnetic properties [54].

2.3.1 Introduction to AISI 316L SS

Grade 316 is the standard molybdenum-bearing grade, second in importance to 304 amongst the austenitic stainless steels. The molybdenum gives 316 better overall corrosion resistant properties than Grade 304, particularly higher resistance to pitting and crevice corrosion in chloride environments.

Grade 316L, the low carbon version of 316 and is immune from sensitization (grain boundary carbide precipitation). Thus it is extensively used in heavy gauge welded components (over about 6mm). There is commonly no appreciable price difference between 316 and 316L stainless steel.

The austenitic structure also gives these grades excellent toughness, even down to cryogenic temperatures. Compared to chromium-nickel austenitic stainless steels, 316L stainless steel offers higher creep, stress to rupture and tensile strength at elevated temperatures [46].

Composition:

Table 2.2 Composition ranges for 316L stainless steel [46].

Grade		C	Mn	Si	P	S	Cr	Mo	Ni	N
316	Min.	-	-	-	-	-	16.00	2.00	10.00	
	Max.	0.03	2.00	0.75	0.045	0.03	18.00	3.00	14.00	0.10

Mechanical Properties:

Table 2.3 Mechanical properties of 316L stainless steel [46].

Grade	Tensile Strength (MPa), Minimum	0.2% Yield Strength (MPa), Minimum	Elongation(% in 50 mm) Minimum	Rockwell hardness (HRB), Maximum	Brinell Hardness (HB), Maximum
316	485	170	40	95	217

Physical Properties:

Table 2.4 Typical physical properties for 316-grade stainless steels [46].

Grade	Density (Kg/m^3)	Elastic Modulus (Gpa)	Mean Co-efficient of Thermal Expansion (µm/m/°C) 0-100 °C	Thermal Conductivity (W/m-K) At 100 °C	Specific Heat 0-100 °C (J/Kg-K)	Electrical resistivity (nΩ.m)
316/L/H	8000	193	15.9	16.3	500	740

Grade Specification Comparison:

Table 2.5 Grade specifications for 316L stainless steel [46]

Grade	UNS No	Old British			Euronorm Name	Swedish SS	Japanese JIS
		BS	En	No			
316L	S31603	316S11	-	1.4404	X2CrNiMo 17-12-2	2348	SUS 316L

Corrosion Resistance:

Excellent in a range of atmospheric environment and many corrosive media-generally more resistant than 304 grade. Subject to pitting and crevice corrosion in warm chloride environments, and to stress corrosion cracking above about 60 °C Considered resistant to potable water with up to about 1000 mg/L chlorides at ambient temperatures, reducing to about 500 mg/L at 60 °C.
316 is usually regarded as the standard "marine grade stainless steel", but it is not resistant to warm seawater. In many marine environments, 316 grade does exhibit surface corrosion, usually visible as brown staining. This is particularly associated with crevices and rough surface finish [51].

Heat Resistance:

Good oxidation resistance in intermittent service to 870 °C and in continuous service to 925 °C. Continuous use of 316 in the 425-860 °C range is not recommended if subsequent aqueous corrosion resistance is important. Grade 316L is more resistant to carbide precipitation and can be used in the above temperature range. Grade 316H has higher strength at elevated temperatures and is sometimes used for structural and pressure-containing applications at temperatures above about 500 °C [51].

Heat Treatment:

Solution Treatment (Annealing) - Heat to 1010-1120 °C and cool rapidly. These grades cannot be hardened by thermal treatment.

Welding:

Excellent weldability by all standard fusion and resistance methods, both with and without filler metals. Heavy welded sections in Grade 316 require post-weld annealing for maximum corrosion resistance. This is not required for 316L [51].
316L stainless steel is not generally weldable using oxyacetylene welding methods.

Machining:

316L stainless steel tends to work harden if machined too quickly. For this reason, low speeds and constant feed rates are recommended [46].
316L stainless steel is also easier to machine compared to 316 stainless steel due to its lower carbon content.

Hot and Cold Working:

316L stainless steel can be hot worked using the most common hot working techniques. Optimal hot working temperatures should be in the range 1150-1260 °C, and certainly should not be less than 930 °C. Post-work annealing should be carried out to induce maximum corrosion resistance [46].
Most common cold working operations such as shearing, drawing, and stamping can be performed on 316L stainless steel. Post-work annealing should be carried out to remove internal stresses.

Hardening and Work Hardening:

316L stainless steel does not harden in response to heat treatments. It can be hardened by cold working, which can also result in increased strength.

2.3.2 Sensitization in AISI 316L SS fabrications

Austenitic stainless steel has good fabrication properties. They also have good weldability and high corrosion resistance. 316L SS is an extra low carbon version of 316 SS which minimizes the carbide

precipitation at the grain boundaries. The sensitization is the major problem that is associated with the welding of these types of stainless steels. Carbide precipitation due to a welding process or heat treatment can cause the occurrence of chromium-depleted zones at the grain boundaries, leading to a phenomenon known as sensitization, in which the depleted zones become the focus of the intense corrosion. Sensitization is the depletion of chromium carbide at the grain boundaries or near the grain boundaries. In the process of welding or heat treatment there is an occurrence of chromium carbide precipitate depletion zone at the grain boundaries which leads to the phenomenon called sensitization. Sensitization leads to the reduction in the corrosion resistance as well as the mechanical properties of the metal. Sensitization promotes the inter-granular corrosion at the heat affected zone [7].

In 316L stainless steel sensitization can be observed in the temperature ranging from 450°C to 900°C and with the increase in thermal aging time extent of sensitization increases.
Sensitization can be controlled by many suitable methods, like rapid cooling the weldment, giving heat treatment like normalizing or annealing. This carbide precipitation can be reduced by lowering the carbon content (below 0.03%wt.) or by the addition of nitrogen and other strong carbide forming elements like titanium, niobium, tantalum etc. But they also have their certain drawbacks. The amount of carbide precipitation can also be reduced by rapid cooling [7].

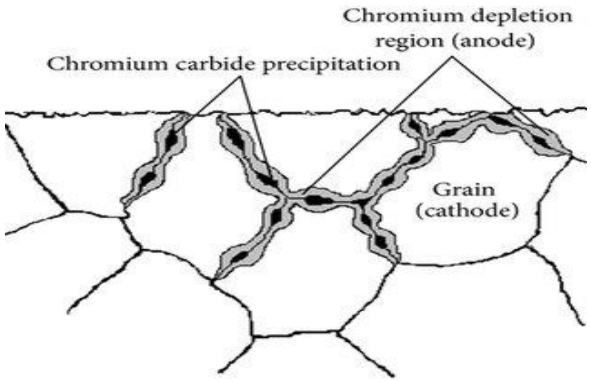

Fig 2.3: *Precipitation of chromium carbide at grain boundary and chromium depleted region [7]*

2.3.3 Kinetics of secondary phase formation

The kinetics of secondary phase formation, in other words, the rate at which secondary phases form on cooling, is a very important factor to consider for the successful annealing and welding of these steels. Regardless of grade, stainless steels must be cooled rapidly enough to avoid the formation of secondary phases. In 316 type chromium carbide is the most likely secondary phase. Chromium carbide is stable and begins to form on cooling at temperatures below about 900°C (1650°F). The rate at which it forms is slow just below 900°C (1650°F), increasing rapidly with decreasing temperature until at about 700°C (1300°F), where it is very high[2].

The kinetics of secondary phase formation can be described by Time Temperature-Transformation (TTT) curves (Figure2.4) for any given alloy. The curves are obtained by first heating test samples to some high temperature (the solution annealing temperature) to dissolve all secondary phases. The samples are then rapidly cooled to an intermediate temperature of interest, held there for various lengths of time, and again rapidly cooled to room temperature to "freeze" the intermediate-temperature structure.

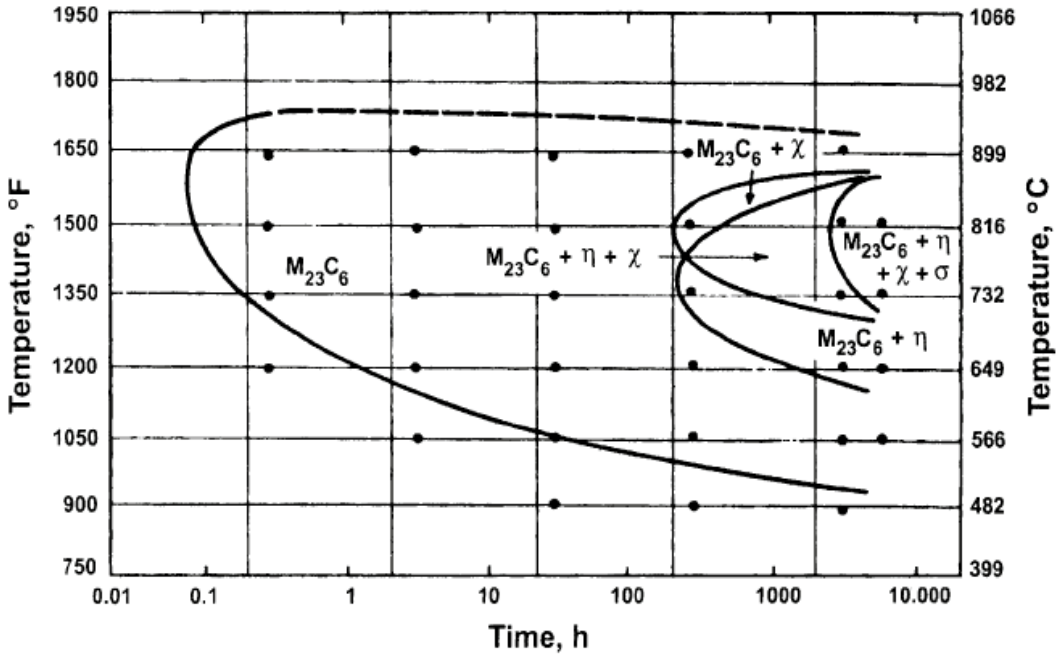

Fig 2.4: *TTT diagram for Type 316L stainless steel with various carbon contents [8]*

From a practical standpoint, the curves show that when annealing or welding these steels with, they must be cooled rapidly below the nose of the curves to avoid sensitization and the associated danger of localized corrosion [2]. Lowering the carbon content extends the available time for cooling, making it easier to avoid sensitization [8].

2.3.4 Applications of 316L stainless steel

Typical applications include:

- Food preparation equipment particularly in chloride environments.
- Pharmaceuticals
- Marine applications
- Architectural applications
- Medical implants, including pins, screws and orthopedic implants like total hip and knee replacements
- Fasteners

2.4 CYCLIC LOADING

2.4.1 Introduction

Failure of mechanical structure involves complex interaction of load, time and environment. The interaction of load, time, and environment along with material selection, geometry, processing and residual stresses creates a wide range of synergistic complexity and possible failure modes in all fields of engineering. Among these failure modes Fatigue is one of the most important and has a large contribution on the most the mechanical failures. Fatigue occurs due to repeated loading. Fatigue failures include more complex components and structures involving ground vehicles, ships, aircraft, and human body implants. Examples are automobile steering linkage, engine connecting rods, ship propeller shafts, pressurized airplane fuselage, landing gears, and hip replacement prostheses [6]. During 1860 August Wohler first started systematic investigation of metal fatigue through laboratory experiments. He also introduced the stress versus life (S-N) curve to illustrate the effect of stress amplitude on the fatigue lives. Later Gerber, Goodman et al. have progressed the systemic study by accounting the effect of mean stress on the fatigue. The systematic studies started this way have continued to reveal various aspect of fatigue with the effort of many researchers [9].

2.4.2 Fatigue stress cycle

Practically mechanical components are subjected to quite diverse loading cycles. In some cases the stress cycling may be simple and repetitive; it also may be completely random. Typical stress cycles are given below:

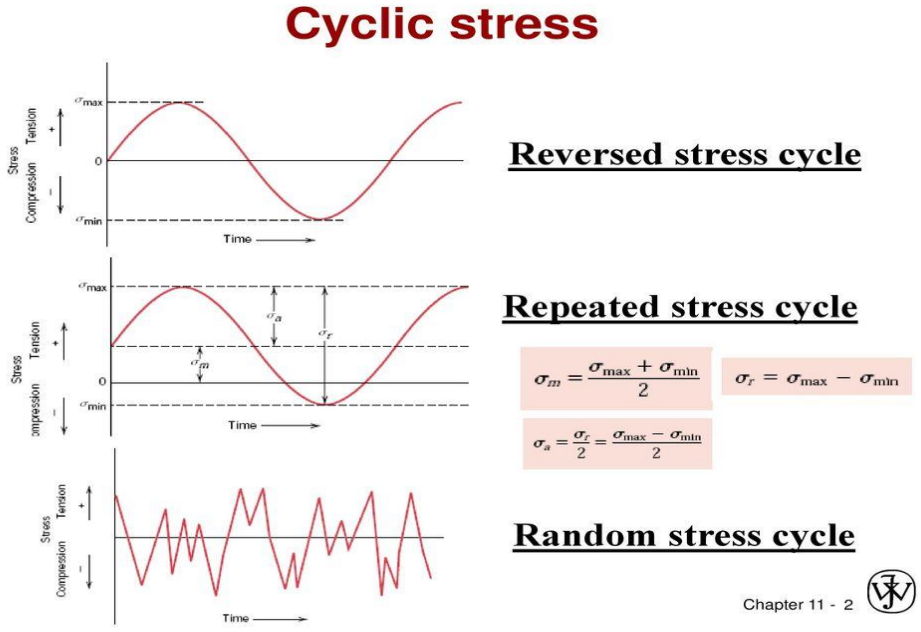

Fig 2.5: *Fatigue stress cycles. (a) Reversed stress cycle of sinusoidal form; (b) Repeated stress cycle of sinusoidal form; (c) Random stress cycle*

2.4.3 Stress Life approach(S-N curve)

The Stress-Life, S-N, method was the first approach used to understand and quantify metal fatigue. It was the standard fatigue design method for almost 100 years. The S-N approach is still widely used in design applications where the applied stress is primarily within the elastic range of the material and the resultant lives (cycles to failure) are long, such as power transmission shaft. The Stress-Life method does not work well in low-cycle fatigue, where the applied strain has a significant plastic component. In low-cycle fatigue the Strain-Life method is more appropriate [10].

S-N curve is concerned with high cycle, where only elastic deformation takes place. With increasing stress the material deforms plastically in a highly localized way. At higher stresses the fatigue life progressively decreased, but the gross plastic deformation makes interpretation difficult in terms of stress [10]. For the low cycle fatigue region tests are conducted with controlled cycles of elastic plus plastic strain instead of controlled load or stress cycles.

2.4.4 Hysteresis loops and the Bauschinger effect

If a metal is cycled to produce plastic deformation in a completely reversed cycling, the resulting cyclic stress strain response will produce a hysteresis loop similar to that of the mechanical parameters associated with the hysteresis loop are indicated on the During the test, either the stress amplitude, $\Delta\sigma/2$, or the total strain, $\Delta\varepsilon$, or the plastic strain, $\Delta\varepsilon_p$, is held constant and the dependant variable is measured during initial loading the stress-strain curve.

Bauschinger effect is observed in cyclic stress strain response of material. This Effect has been defined as “the phenomenon by which plastic deformation increases yield strength in the direction of plastic flow and decreases it in other direction”. The effect is graphically illustrated by the shape of hysteresis loop of Figure 2.6 which shows that on unloading, plastic deformation begins at a lower backward stress, σ_B, than reached in the forward direction, σ_F [10].

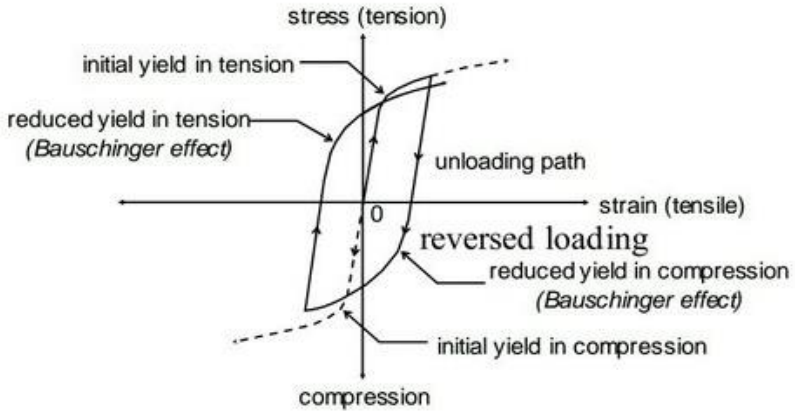

Fig 2.6: *Hysteresis Loop [10]*

2.4.5 Cyclic hardening and softening

Since plastic deformation is not completely reversible, modifications to the structure occur during cyclic straining and these can result in changes in the stress-strain response. Depending on the initial state a metal may undergo cyclic hardening, cyclic softening, or remain cyclically stable. It is not uncommon for all three behaviors to occur in a given material depending on the initial state of the material and the test conditions. Figure2.7 illustrates cyclic hardening and softening for strain controlled cycling. It is worth noting how the hysteresis loops change with successive cycles. Note that with cyclic stressing under stress control the behavior would be reversed. Cyclic hardening would lead to a decreasing peak strain with increased cycles and cyclic softening would lead to a continually increasing strain range and early fracture [11].

The number of cycles a material would dwell within the fatigue Hardening/softening process depends on various factors. One of the most important parameters is the cross slip ability of the material. The ability of a material to cross slip can be roughly divided into two groups: wavy-slip materials like Cu, Al, Ni, Fe, carbon steels, etc. and planar-slip materials like brass, austenitic stainless steels, Fe-Si alloys, etc. Wavy slip basically can be described as easy cross slip while planar slip indicates a rare and difficult cross slip. This is related to the stacking - fault energy (SFE): in general the higher the stacking- fault energy the easier and more frequent the cross slip, and more markedly one will see wavy slip bands on the primary slip planes. In general, the number of cycles spent in hardening/softening is lower for wavy-slip materials than for planar-slip materials.

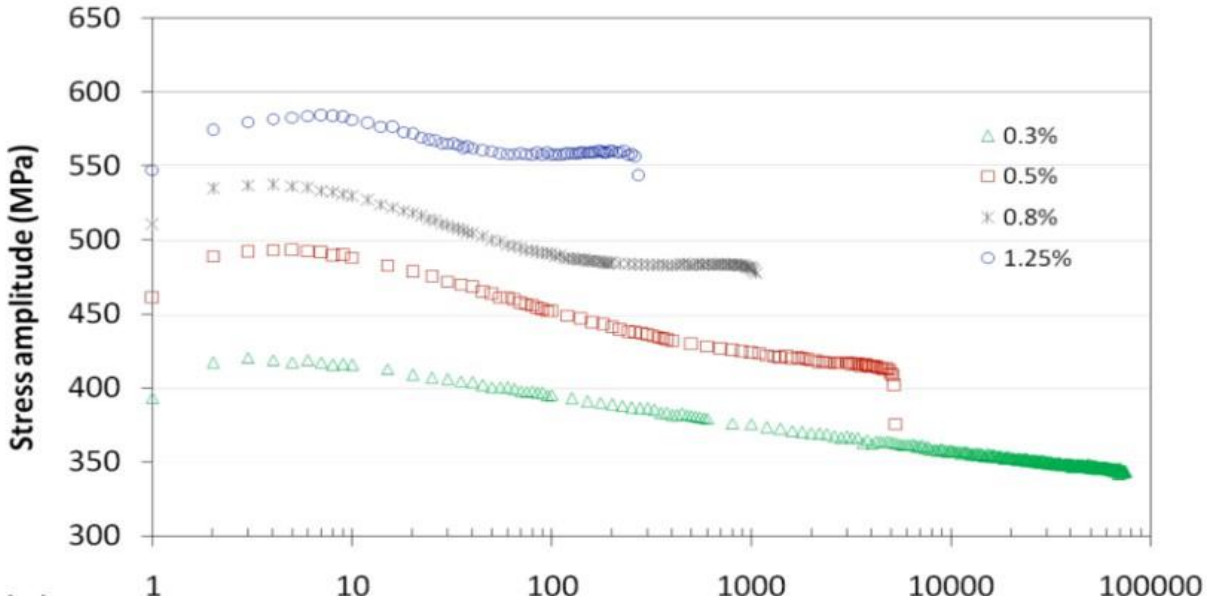

Fig 2.7: *Cyclic hardening and softening behaviour for AISI 316L [11]*

Rohatgi et al. [12] have correlated between the SFE, dislocation density and shock strengthening in schematic diagram as shown in Figure 2.8. The shock deformed SFE materials are unable to store sufficient dislocation density (compared to high SFE material) since part of the shock strain is accumulated by twinning and partly due to the enhanced Bauschinger effect in low SFE materials is enhanced due to the difficulty of cross slip and indirectly through the effect of twins.

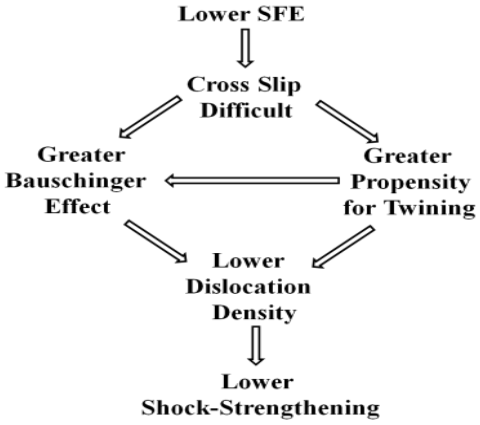

Fig *2.8:* *Schematic diagram of the relationship between stacking fault energy, dislocation density and shock-strengthening [12]*

Stacking Fault energy greatly affects the work hardening behavior of FCC metals or alloys in simple tension or compression test. Asgari et al. [13] and EI-Danaf et al. [14] have reported the variation of work hardening rate with true strain. According to their observation the four stages work hardening behavior occur in case of low stacking fault energy material instead of higher stacking fault energy material as schematically shown in the Figure 2.9. The four stages work hardening behavior has been discussed in the following section.

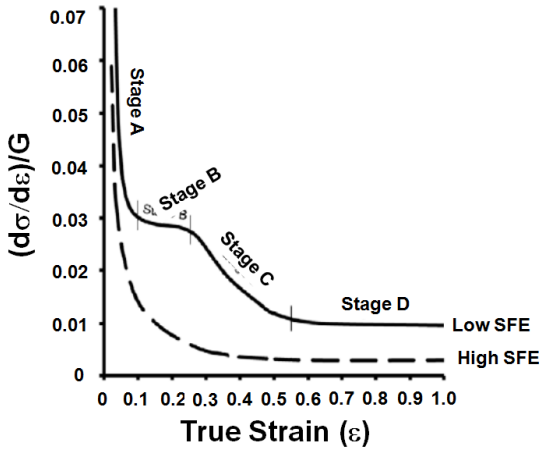

Fig 2.9: *Schematic representation of four stages strain/work hardening behavior of both lower stacking fault energy (SFE) and higher stacking fault energy (SFE) material [14]*

Stage A hardening starts instantly after yielding of the material and is characterized by a gradual decrease in hardening rate. The nature of this stage is not unambiguous. The elasto-plastic transition and development of slip systems in the elastically deformed crystals is considered to be the main cause of the occurrence of this stage of hardening [15]. In stage B the work hardening rate remains at a relatively constant value and a plateau region is formed. This stage of hardening includes the effect of mechanical twining as deformation twining leads to the reduction in slip length. The stress range of Stage B decreases with increasing SFE value and may even vanish for high SFE FCC metals or alloys.

Stage C hardening is characterized by breakdown of the constant hardening rate observed in Stage B hardening. This phenomenon is explained by dynamic recovery mechanism and has been attributed to the activation of cross-slip processes [16]. The stress and strain level corresponding to the transition from Stage B to Stage C was found to be inversely dependent on temperature and stacking fault energy [15].

Stage D hardening is explained based on saturation of the hardening rate to a finite value. This value is different from saturation for higher SFE FCC metals and alloys, in which the work hardening rate approaches to zero[13,14]. It has been suggested that activation of a secondary twining system further reduces slip lengths and causes additional hardening.

Rohatgi et al [12] also reported that work hardening rate is relatively higher for lower SFE metals or alloys at higher strain level than the higher SFE metals or alloys suggesting that these metals or alloys have not reached its saturation stress and have the potential for further strain hardening. Another cause of having higher work hardening rate for lower SFE metals is that lower SFE metals make it easier for a full dislocation to split into two partials with a wider stacking fault ribbon between them which makes it difficult for the full dislocation to cross slip or climb when it encounters a barrier, which hinders the dislocation recovery via cross slip and climb [17].

During the cyclic plastic deformation behavior the shape of hysteresis loop changes from cycle to cycle throughout the fatigue life for every material. The change of such hysteresis loops is depending upon the cyclic softening or cyclic hardening behavior of the materials. The cyclic hardening or softening behavior during either stress control or strain control is schematically shown in the Figure 2.10. In case of constant stress controlled symmetric cyclic loading the cyclically hardening and softening response can be expressed as the decrease of peak strain and the increase of peak strain respectively in every cycle up-to the failure of the material. While in case of constant strain controlled symmetric cyclic loading the cyclically hardening and softening response can be expressed as the increase of peak stress and decrease of peak stress respectively in every cycle up-to the failure of the material [17]. In some cases cyclic saturation appears after cyclic hardening or softening stage where the hysteresis loop remains stable and constant peak stress or constant peak strain is maintained.

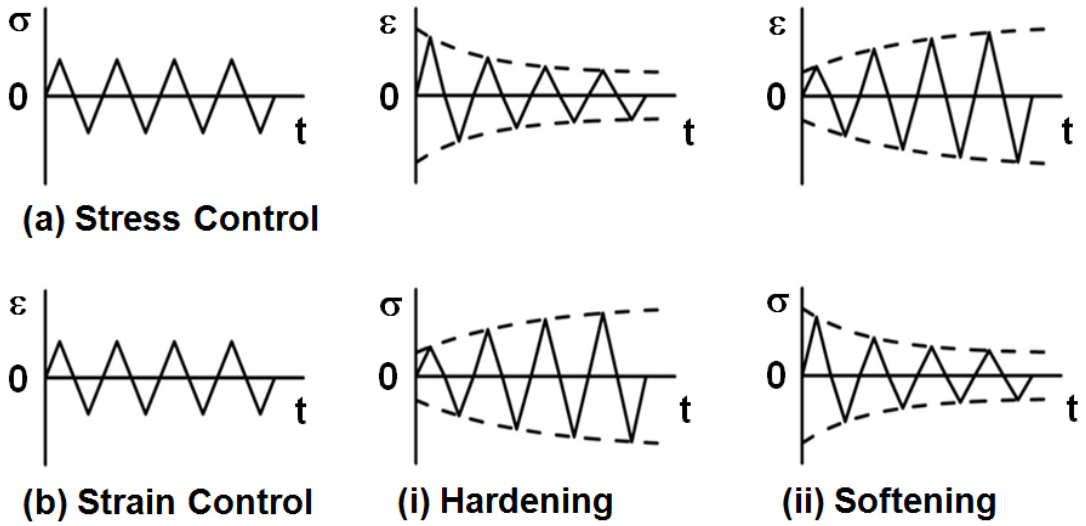

Fig 2.10: *Schematic representation of hardening and softening behavior during (a) stress controlled and (b) strain controlled cyclic deformation [17].*

2.5 RATCHETING BEHAVIOR OF DIFFERENT SFE FCC METALS

2.5.1 Introduction

Structural components are often subjected to stress cycling in elasto-plastic domain with non-zero mean stress resulting in the accumulation of inelastic strain cycle-by-cycle in the direction of mean stress. Such accumulation of inelastic strain cycle-by-cycle during this asymmetric cyclic loading is called ratcheting [52]. During the ratcheting deformation, in addition to cyclic damage an additional damage occurs due to the accumulation of inelastic strain. Thus the ratcheting deformation is one of the important factors which should be considered in design of structural components subjected to asymmetric cyclic loading. Several authors have been extensively studied the ratcheting behavior of FCC metals by experimentally and by modeling. The lots of factors are involved in the ratcheting strain accumulation process such as mean stress, stress amplitude and stress ratio, different loading histories, different hardening and softening characteristics of different materials at different heat treated conditions and ultimately the failure by interaction of fatigue process and excessive strain. Some of the affecting factors involved in the ratcheting processes have been explained in this section. Changes in mechanical properties due to prior ratcheting deformation and determination of cyclic hardening/softening factors have been explained in this section [52].

2.5.2 Characteristics of Ratcheting

Due to presence of mean stress in asymmetric cyclic loading, non-closed stress strain hysteresis loops develop as a consequence of difference in plastic deformation in the forward and reverse cyclic deformation. Such cyclic plastic strain difference in loading and unloading parts of stress cycles causes the specimen to elongate or compress depending upon whether the mean stress is

positive or negative. Figure 2.11(a-b) describes the schematic representation of hysteresis loop during symmetric and asymmetric cyclic loading [52]. The accumulation of inelastic strain at every cycle during asymmetric cyclic loading is schematically represented in Figure 2.11(b). The most widely used method for measuring ratcheting strain is given by

$$\varepsilon_r = \frac{1}{2}(\varepsilon_{\max} + \varepsilon_{\min}) \qquad \textbf{(2.1)}$$

Where ε_{max} and ε_{min} are maximum and minimum strain per cycle respectively and they increase in each cycle depending upon the magnitude of applied mean stress and stress amplitude. The ratcheting strain accumulation per cycle can be calculated by [52]

$$\delta\varepsilon = {}_{n+1}\varepsilon^{peak} - {}_{n}\varepsilon^{peak} \qquad \textbf{(2.2)}$$

Where ${}_{n}\varepsilon^{peak}$ and ${}_{n+1}\varepsilon^{peak}$ are the peak strain produced in n^{th} and $n+1^{th}$ cycles respectively. The ratcheting strain accumulation occurs in the direction of mean stress.

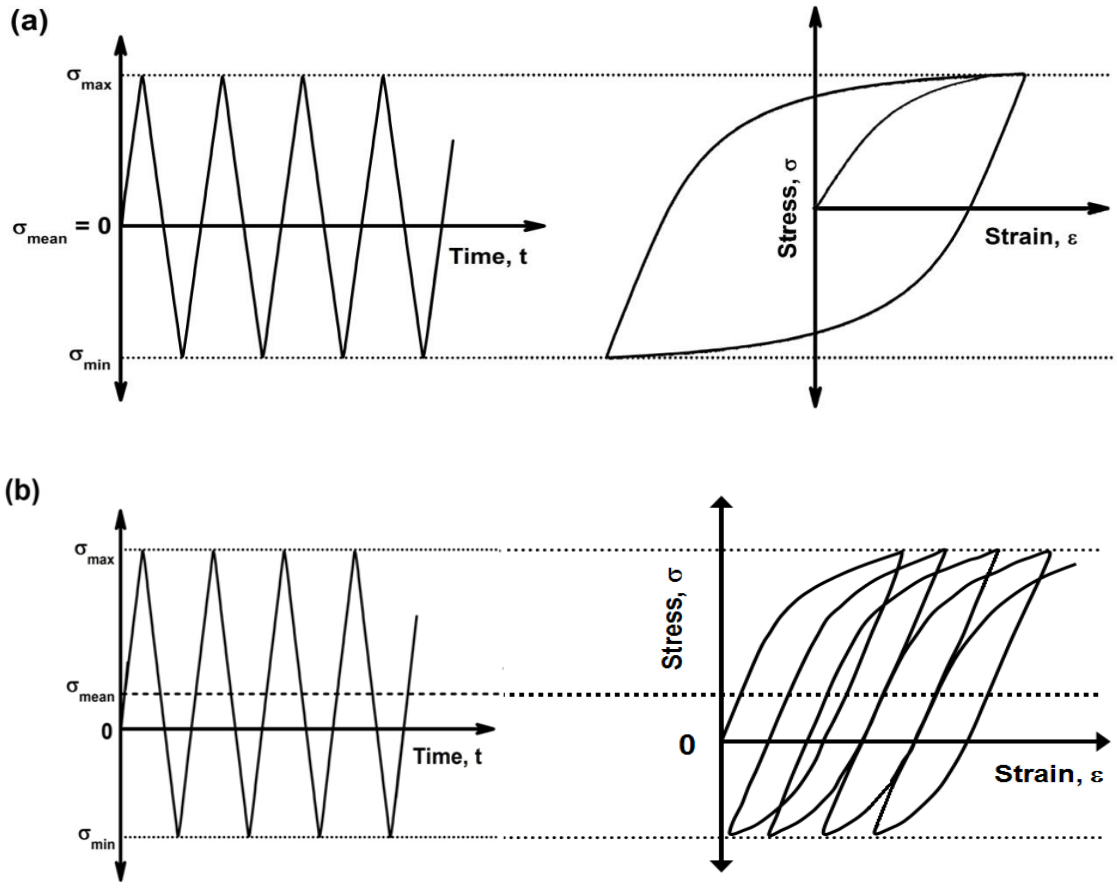

Fig 2.11: *Schematic diagram showing translation of hysteresis loop at (a) zero mean stress and (b) positive mean stress*

During asymmetric cyclic loading with positive mean stress on elasto-plastic materials may have three possible asymptotic responses after a certain number of cycles as schematically represented in the Figure 2.13. Elastic shake down occurs only when elastic deformation takes place even after a certain number of stress cycling. Similarly plastic shake down occurs when closed steady plastic hysteresis loops take place after certain number of stress cycling. The elastic shake down stress cycling will lead to high cycle fatigue failure while plastic shakedown cycling will lead to low cycle fatigue failure [52]. The plastic shakedown occurs due to mainly formation of stable dislocation structure after a certain number of stress cycling. This hinders further ratcheting strain accumulation at lower maximum stress value and closed steady plastic hysteresis loops are formed. The ratcheting deformation takes place when the rate of deformation per cycle is constant. In this case the constant ratcheting rate is maintained due to two competitive effects, one is cyclic hardening of the material and another one is cross sectional area reduction due to accumulation of tensile ratcheting strain which results into increment of true stress amplitude and true mean stress. The ratcheting and shakedown are sequential mechanisms and a pure ratcheting failure will occur only when the plastic shakedown does not occur.

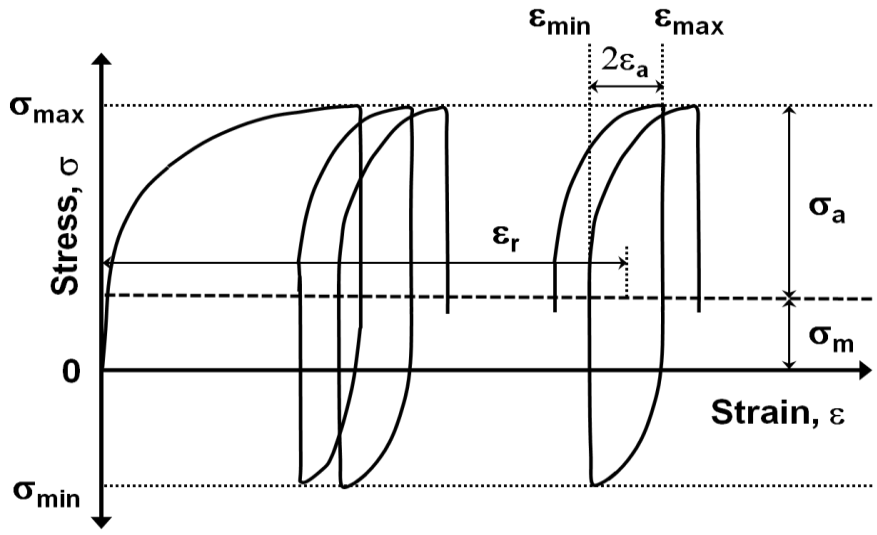

Fig 2.12: *Schematic representation for calculation of ratcheting strain*

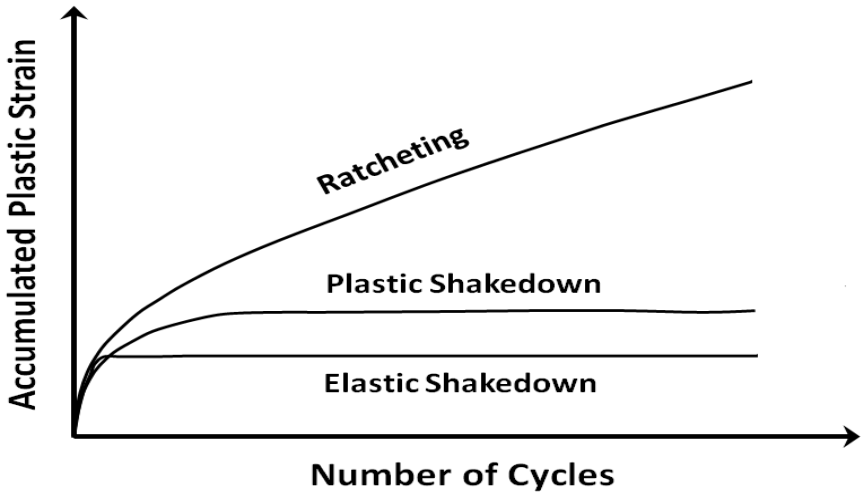

Fig 2.13: *Possible phenomena of cyclic plasticity under asymmetric cycling loading condition [47].*

During asymmetric cyclic loading, ratcheting strain accumulation occurs in different stages. Generally, under engineering stress control conditions ratcheting strain accumulation occurs in three different stages. Ratcheting strain rate i.e. rate of strain accumulation per cycle in different stages is different as schematically represented in Figure 2.14.In stage I the ratcheting strain rate decreases rapidly within first few cycles. In stage II the ratcheting strain rate remains constant and finally it start to increase in stage III. The stage II is known as steady state ratcheting deformation. The attainment of steady state ratcheting rate in stage II can be explained by formation and distribution of dislocation associated with cyclic deformation. After annihilation of dislocation during reverse cycling, the remnant dislocations initially form tangles and with further cycling dislocation cell structures are formed [18]. After certain number of cycles, depending on the accumulated ratcheting strain, the newly generated dislocations assume a relatively stable configuration which leads to the initiation of steady state ratcheting rate. In engineering stress control mode of asymmetric cyclic loading the ratcheting strain rate in stage III increases up-to complete failure of the specimen. In this case the effective true stress on the material increases with increase in ratcheting strain due to the specimen elongates with accumulation of inelastic strain. In this case along with the hardening and softening behavior of a material the geometrical softening also takes place. However such geometrical softening does not occur during true stress control asymmetric cyclic test. As a result stage III deformation does not occur in case of true stress control asymmetric cyclic test [19,20].

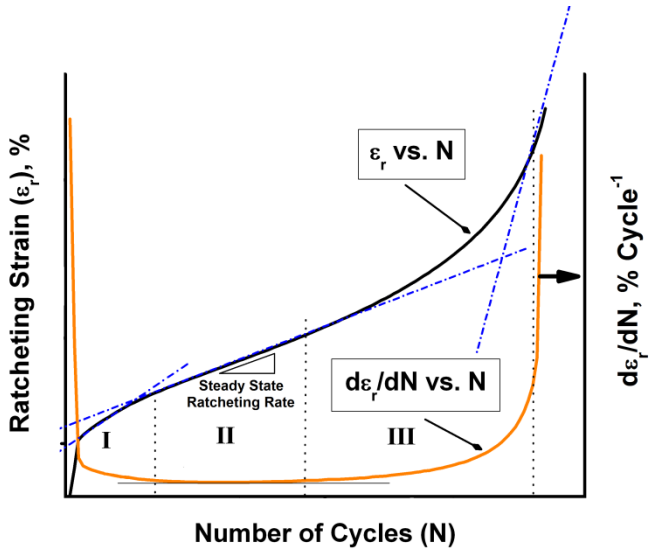

Fig 2.14: *Schematic representation of ratcheting strain accumulation and corresponding ratcheting strain rate evolution with number of cycles [19].*

Regarding the importance of mean stress and stress amplitude effect on the performance of structural components subjected to asymmetric cyclic loading in elasto-plastic domain many investigations have been carried out for about last three decades to understand uniaxial and multiaxial ratcheting behavior of different materials like: IF steel [21], SA 333 Gr. C-Mn Steel [20], SA 333 Steel [22], SS 304 Stainless Steel [23], SA333 Gr. 6 steel [24], Inconel 718[25], etc. The three stage ratcheting rate evolution has been studied by some of the above researchers and the variation has been looked into with respect to the mean stress and stress amplitude. But the effect of mean stress and stress amplitude on average steady state ratcheting rate has not been clearly reported by these researchers. As number of cycles to failure and ratcheting strain evolution during stress-control cyclic loading is dependent on the ratcheting strain rate, it is expected that there should be a relation between average steady state ratcheting strain rate and number of cycles to failure irrespective of stress combinations.

2.5.3 Effect of Stress Parameters on Ratcheting Behavior

Generally, effects of stress amplitude (σ_a) and mean stress (σ_m) on ratcheting behaviors are studied in two different ways: (1) interaction between stress amplitude and mean stress and (2) interaction between maximum stress and stress ratio. During asymmetric cyclic loading either at constant stress amplitude or constant mean stress, the maximum stress (σ_{max}) and minimum (σ_{min}) stress in the cyclic waveform vary depending upon the mean stress or stress amplitude. When the mean stress is positive, σ_{max} is always greater than $|\sigma_{min}|$ and σ_{min} value is always negative. So the mobile dislocation density at σ_{max} is more than that of σ_{min} point. During the reverse compressive unloading part of the stress cycle, only a fraction of dislocation that forms during the tensile loading

direction gets annihilated. As a result after every asymmetric cyclic loading, there will be a net storage of mobile dislocations in substructure of the material. As amount of plastic deformation is related to mobile dislocation density, the ratcheting strain evolution in every cycle will be higher for higher σ_{max} resulting from either the increase of stress amplitude or increase of mean stress [21-23].

In most of the cases it has been reported that at constant stress amplitude level ratcheting strain evolution increases and ratcheting life decreases with increasing the mean stress level. Such observation is true for almost all materials with different hardening/softening characteristic [21-23, 25-27]. They also reported the pronounced effect of stress amplitude on ratcheting strain evolution as well as ratcheting life at constant mean stress level. Increasing the stress amplitude at constant mean stress level both the ratcheting strain evolution and ratcheting strain rate increases. As the ratcheting strain rate increase with increase in stress amplitude at constant mean stress level, the ratcheting life decreases. It has also been reported that the effect of stress amplitude on ratcheting strain, ratcheting strain rate evolution and ratcheting life is more compared to the effect of mean stress.

In order to understand the effect of mean stress and stress amplitude on ratcheting behavior, Dutta et al.[21] have carried out the details investigation on ratcheting strain in IF steel. They have carried out the ratcheting test up-to 100 cycles at different combination of mean stress and stress amplitude using triangular waveform at strain rate of 50 MPa sec^{-1}. They have reported that with increase in σ_m at constant σ_a value the maximum stress (σ_{max}) increases and such increase in σ_{max} would induce higher extent of plastic deformation of the material and as a consequence ratcheting strain accumulation increases. This phenomenon has been correlated with the formation of dislocation structure within the material, the number of dislocation generated during loading cycle is higher compared to that of unloading cycle. But during the load reversal only a part of generated dislocations get annihilated and the remaining dislocations act as residuals in the substructure of the material. As a result higher ratcheting strain accumulation takes place at either higher mean stress or stress amplitude levels. As discussed above, with increase in either σ_m or σ_a, number of remnant dislocation increases, results to increase in ratcheting strain rate with increase in either σ_m or σ_a value.

In case of effect of stress ratio ($R = \sigma_{min}/\sigma_{max}$) at constant maximum stress level, it is necessary that the stress ratio must be sufficiently negative for ratcheting to occur [28]. As discussed above the remnant dislocation density after annihilation during reversals of every cycle depends on the applied maximum stress and minimum stress amplitude. It has been mentioned earlier that the ratcheting strain evolution in every cycle will be higher for higher σ_{max} value resulting from either the increase of stress amplitude or mean stress value. Therefore it can be said that there should be effect of stress ratio on ratcheting behavior at constant σ_{max} value. Several researchers have reported

that the stress ratio influences the ratcheting strain evolution as well as ratcheting life at constant maximum stress level [23, 29-33]. Increasing the stress ratio at constant maximum stress means decreasing stress amplitude and increasing mean stress by the same amount. As pointed out earlier the effect of stress amplitude is more compared to mean stress. Therefore, increase in stress ratio at constant maximum stress level results in decreasing ratcheting strain. Some of the above researchers also pointed out that ratcheting life rapidly increases with stress ratio at constant maximum stress and the ratcheting life with higher maximum stress is shorter than that with small one when the stress ratio is same. De et al. [30] also reported that with increase of stress ratio at constant maximum stress, the dislocation-dislocation interaction increases with increase of net dislocation storage leading to harden the material.

2.5.4 Engineering and True Stress Control Ratcheting Behavior

For true stress change along with the plastic strain accumulation, change in cross-sectional area must to be considered. The actual deformation behavior can only be understood from true stress and true strain. Therefore, the true stress controlled experiment has to be carried out where substantial change in cross sectional area taken into account [52]. Besides, the actual deformation point of view in true stress controlled ratcheting, the engineering stress controlled ratcheting deformation behaviour is also equally important from engineering point of view because in practical there is no provision to measure and control the true stress.

The ratcheting tests were effectively carried out by feedback of strain accumulated during testing for calculation of loads so as to maintain a constant true stress value [52]. For true stress control tests, failure originated from initiation and growth of fatigue crack. It has been observed that most specimens failed through necking in engineering stress control test. The obtained Ratcheting life in engineering stress control ratcheting test was very low compared to true stress control ratcheting tests [52]. It has also been observed in case of engineering stress control ratcheting tests with positive mean stress that the specimen elongated in the direction of mean stress along with the reduction in cross sectional area. Hence in that case true stress amplitude as well as effective maximum stress increased with the number of cycles as schematically represented in Figure 2.15. But in case of true stress control mode of ratcheting tests the true stress amplitude as well as effective maximum stress remained constant with number of cycles, Figure 2.15. It has been analysed by many authors that as the effective load or true stress amplitude increased with number of cycles in case of engineering stress control tests, the number of cycles to attain same amount of ratcheting strain in engineering stress control ratcheting tests was less compared to true stress control ratcheting tests [52].

So it can be said that with the continuous enhancement of the true stress levels there would be continuous change in the material deformation behaviour. Eventually, it would make it difficult to interrupt material performance in engineering stress control tests. Therefore it can be noted that with

the increase in true stress amplitude and true mean stress would ultimately lead to continuous change in cyclic plastic deformation pattern. The deviation of true stress amplitude from engineering stress amplitude can be observed for even small accumulation of ratcheting strain in case of engineering stress control, but the effect would be more prominent for considerable accumulation of ratcheting strain.

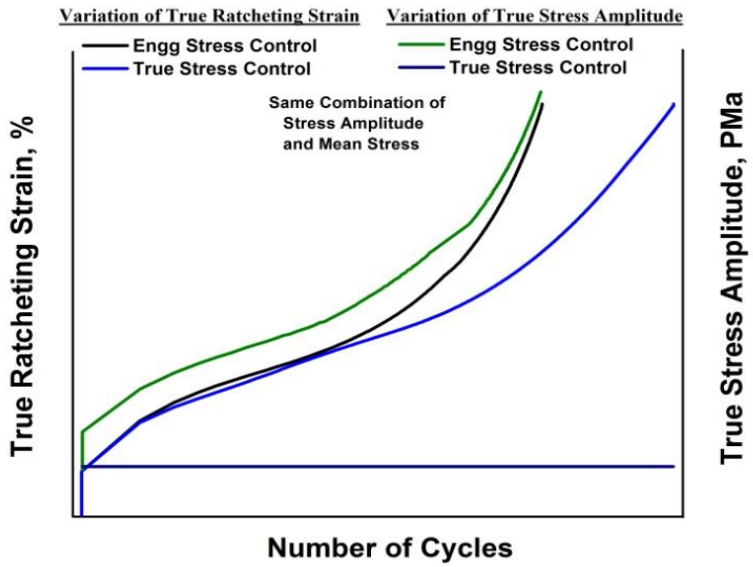

Fig 2.15: *Schematic diagram of variation of true ratcheting strain and true stress amplitude for both engineering and true stress control mode of ratcheting tests.*

2.5.5 Cyclic Plasticity under Ratcheting

Evolution of ratcheting strain in asymmetric cyclic deformation depends on cyclic hardening and softening characteristics of material. Several investigators have studied the evolution of cyclic plasticity during ratcheting deformation of different materials [22, 34]. They have reported that the cyclic plasticity, which is represented by plastic strain amplitude, depend greatly on both mean stress and stress amplitude. It has been reported that for cyclically softening material like tempered 9%Cr–1%Mo[34] steel and tempered 42Cr-Mo steel produce higher strain amplitude response with increased mean stress at constant stress amplitude level. But in case of cyclic hardening material like SA 333[22], SS 304[23] and ASS 304LN [27] does not exhibit similar effect of mean stress on strain amplitude response. They have reported that with increase in mean stress at constant stress amplitude level the plastic strain amplitude decreases. This type of different behavior is not observed in case of varying stress amplitude. Strain amplitude response is always found to increase with increasing stress amplitude in stress cycling at constant mean stress level. Such type of variation is true for all types of material as mentioned earlier [22, 34]. It has also reported that similar increase in plastic strain amplitude has been noticed with increase in negative stress ratio during at constant maximum stress asymmetric cycling.

2.5.6 Post Ratcheting Tensile Behavior

The importance of engineering and true stress control ratcheting behavior of metallic materials and effect of mean stress (σ_m), stress amplitude (σ_a) and stress ratio (SR) on ratcheting behavior i.e. ratcheting strain, ratcheting strain rate and ratcheting life have been discussed in the earlier section. Most of existing investigations on ratcheting behavior of metallic materials are related to the mechanics of cyclic loading parameters, but these reports have not carefully described the micro-mechanism of ratcheting in material. In case of ratcheting, the change in material properties occurs due to combined effect of cyclic deformation and accumulation of ratcheting strain. Therefore it is expected to cause variation in metallic post-ratcheting tensile properties. Such post ratcheting tensile behavior has been studied earlier by Dutta et al. [35, 36]. Dutta et al. [35] have studied the post ratcheting tensile behavior of Aluminium alloy by substructure variation during ratcheting and corresponding variation of post ratcheting tensile properties. From the above discussion regarding the effect of mean stress, stress amplitude and maximum stress on ratcheting strain accumulation, increase in maximum stress by increasing either stress amplitude or mean stress, extent of plastic deformation increases and such phenomenon can be correlated to the dislocation substructure of material. It has also been discussed that after annihilation of dislocation during reverse loading of every cycle the remnant dislocations act as residual in the substructure of the material. It is well known that higher is the remnant dislocation density in the material, higher is the accumulation of plastic strain and vice-versa. In other words it can be said that higher the accumulation of plastic strain results in higher remnant dislocation density. Therefore, after accumulation of certain ratcheting strain the remnant dislocation density and dislocation substructure are different due to different applied value of mean stress and stress amplitude. This results in variation of post–ratcheting tensile properties.

Dutta et al[35] have observed that the tensile strength of ratcheted specimens are higher than that of corresponding as received or annealed ones and these values increase with increase in either mean stress or stress amplitude. Simultaneously tensile ductility of ratcheted specimen is lower compared to the as received and as annealed condition. While De et al. [36] have reported the linear variation of post ratcheting tensile properties with prestrain in Ti-stabilised IF steel.

To explain mean stress, stress amplitude and stress ratio dependent cyclic hardening and enhancement of post ratcheting tensile properties, plastic strain amplitude and plastic strain energy variation with number of cycles are more important as both the plastic strain amplitude and plastic strain energy are damaging parameter in cyclic plastic deformation. Decrease in cyclic plastic strain amplitude represents the cyclic hardening of the material. But in case of stress control asymmetric cyclic hardening, the calculation of plastic strain range is not similar to that of the symmetric cyclic loading due to non-closing nature of hysteresis loops as discussed in section 2.4.5. In this regard Ni

et al. have studied the effect of pre-strain on cyclic hardening/softening behavior in iron based alloy on the basis of net plastic strain and total plastic strain variation with number of cycles. Pokluda et al.[37] also have reported the effect of mean stress on net plastic strain range and total plastic strain range at constant higher stress amplitude level, increase in mean stress results in decrease the net plastic strain range. Hardening or softening of materials caused by asymmetric cyclic loading can also be expressed in terms of variation of plastic strain energy with number of cycles as discussed in the previous section. But plastic strain amplitude and plastic strain energy variation can't be taken as universal parameter to represent cyclic hardening/ softening behavior in case of asymmetric cyclic loading condition..

2.5.7 Role of Stacking Fault Energy on Ratcheting Behavior

In the earlier section it has been mentioned that the ratcheting behavior depends greatly on types of materials i.e. different crystal structure or different value of stacking fault energy (SFE) material. In this regard Kang et al.[38] have experimentally observed the uniaxial ratcheting behavior of different values of stacking fault energy materials. They have reported that in case of stress control asymmetric cyclic loading condition the ratcheting strain does not decrease with decreasing value of stacking fault energy, but decrease with decreasing extent of cyclic hardening of the material, shown in Figure 2.16. From this figure it is clear that the ratcheting behavior of pure Aluminium is most significant among the three FCC metals as its extent of cyclic hardening is the lowest one. But pure Copper presents the weakest ratcheting behavior due to its strongest cyclic hardening among the three FCC metals. Therefore, it can be said that quicker the formation of stable dislocation structure or dislocation cell, weaker the ratcheting behavior in the material.

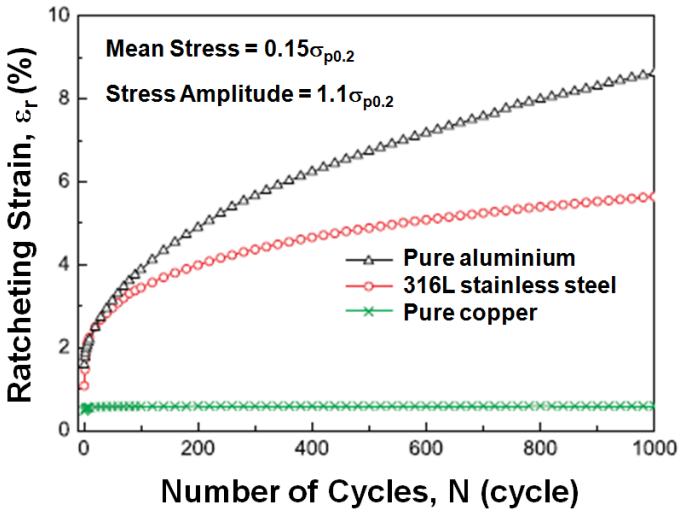

Fig 2.16: *Comparison of uniaxial ratcheting results of three different FCC metals with different values of stacking fault energy [38].*

2.5.8 Failure during Ratcheting

In case of ratcheting deformation behavior in addition with the accumulation of ratcheting strain, cyclic fatigue damage also act independently or synergistically in the test specimen. It is known that fatigue damage occurs following crack initiation and propagation without any gross plastic deformation in the test specimen. But ratcheting deformation occurs by accumulation of plastic strain in every cycle and the test specimen failed by excessive elongation or complete failure following necking before the advent of fatigue cracking or fracture. Stress control asymmetric cyclic loading may results in elastic shakedown which would lead to high cycle fatigue failure (HCF). Other material response like plastic shakedown would lead to low cycle fatigue failure.

Stress control symmetric cyclic life can be predicted by Basquin relationship [10].

$$\frac{\Delta\sigma}{2} = \sigma_a = \sigma_f^{'}(2N_f)^b \qquad \textbf{(2.3)}$$

Where, $\sigma_f^{'}$ is the fatigue strength coefficient which is equal to the true fracture strength in monotonic tension test and b is the fatigue strength exponent which is in the range of -0.05 to -0.12.

The failure life in case of asymmetric stress cyclic loading is changes from that of failure life in symmetric stress cyclic loading. In this regard to incorporate the effect of mean stress various models have been proposed as for example Goodman equation [39], modified Goodman equation[40] and Smith–Watson–Topper (SWT) parameter based equation[41]. General validity of Basquin relationship is within the high cycle fatigue regime where elastic strain dominant fatigue failure is observed. Kwofie and Chandler[42] have shown that stress–life (S–N) curve or relation is not limited to high cycle fatigue regime but has potential application in the low-cycle fatigue regime as well, especially under conditions where cyclic creep–fatigue interaction is eminent. For predicting the ratcheting-fatigue failure life various modification of the Basquin relationship has been proposed. Most this modification relies on the replacing the stress amplitude with an equivalent stress amplitude, similar to Goodman equation, incorporating the mean stress parameter in the function with various form. In some approach strain amplitude or ratcheting strain rate has been incorporated in the function [22, 25, 43, 44].

2.5.9 Fatigue Life in Ratcheting

The fatigue lives of the steel under asymmetrical uniaxial cyclic loading for various combinations of mean stress, σ_m and stress amplitude, σ_a are shown in Fig. 2.17(a) to (b). It was seen from Fig. 2.17(a) that the fatigue life of the steel decreased initially when σ_m level increased from 63 to 94 MPa. This aspect is to some extent in line with those obtained by Xia et al. and Rider et al for low-alloy steel and low carbon steel, respectively, but completely dissimilar from that of

SS304 stainless steel. It is quite interesting to see that after initial decrease in fatigue life, once mean stress level was further raised from 94 to 188 MPa, the steel exhibited marginal but continual improvement in fatigue lives despite a fair amount of increase in ratcheting strain. Such extension of fatigue life in the presence of tensile mean stress is not so uncommon in the event of ratcheting. However, this phenomenon has been termed as ‘‘mean stress-induced hardening’’ in which higher mean stress lowers plastic strain amplitude associated with lesser crack initiation and slower crack growth rate. Paul et al. [27] also argued that the increasing level of mean stress results in decrease in both plastic strain amplitude and plastic strain energy and the systematic decrease of both these parameters starts occurring from the very first cycle as a consequence of which fatigue life increases. Beneficial effects of tensile mean stress on the ratcheting fatigue life of stainless steel, carbon steel, polycrystalline nickel and polycrystalline copper are also well documented in the literature. Since cyclic deformation-induced crack initiation and propagation is largely controlled by the dislocation dynamics in the substructure of the material, the variation of fatigue life with the increase in σ_m level is, therefore, undoubtedly attributed to the interplay of the dislocations in the material. Similarly, the effect of stress amplitude on the ratcheting lives of the investigated rail steel at constant σ_m is shown in Fig. 2.17(b). This figure shows that the ratcheting life of the steel was greatly influenced by varying stress amplitude, i.e., increasing stress amplitude significantly shortened the life of the specimens. The highest ratcheting life was obtained at the lowest stress amplitude level.

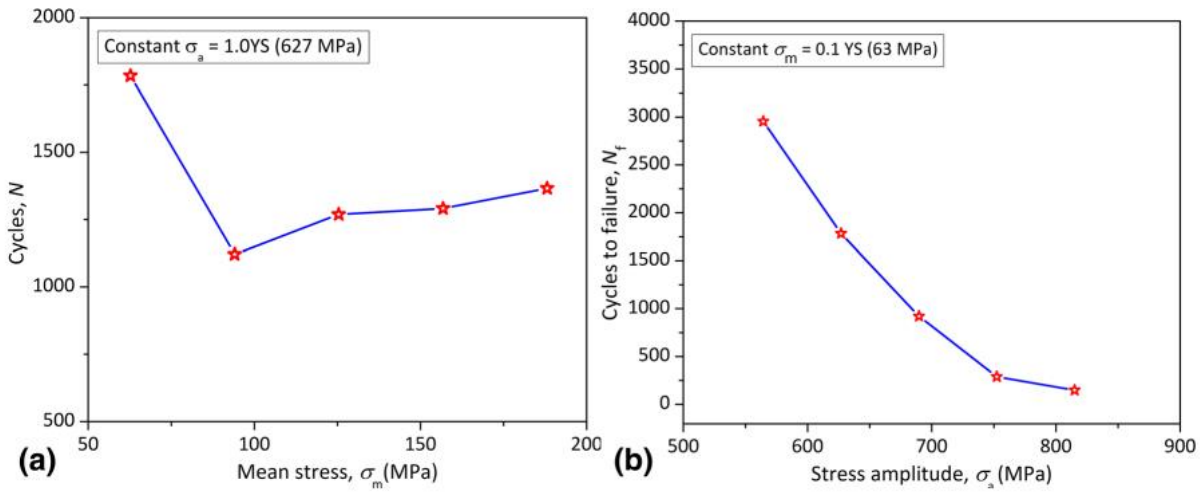

Fig 2.17: *Variation in fatigue life of the investigated rail steel as a function of (a) σ_m at constant σ_a and (b) σ_a at constant σ_m [27].*

This implies that the fatigue life of the material under asymmetrical cyclic stressing is appreciably controlled by applied stress amplitude. However, the effect of increasing σ_a on

ratcheting strain evolution was observed to be much greater than that of σ_m. Earlier investigations carried out by Kang et al. on 304 stainless steel and Sivaprasad et al. on SA333 Gr. 6 C-Mn steel also demonstrated that the effect of stress amplitude was much higher than the effect of mean stress on ratcheting strain evolution resulting in lower ratcheting lives.

2.6 CHARACTERISATION OF TENSILE BEHAVIOUR

2.6.1 Introduction

Tension test is widely used to provide basic design information on the strength of the material and as an acceptance test for the specification of materials. In the tension test a specimen is subjected to a continually increasing uniaxial tensile force while simultaneous observations are made of elongation of the specimen. The shape and magnitude of the stress-strain curve of a metal depends on its composition, heat treatment, prior history of plastic deformation, and the strain rate, temperature, and state of stress imposed during testing.

The primary area of analysis has been the strain hardening behavior of material in which the hollomon and Ludwik analysis has been performed.

2.6.2 SEM fractographical characteristics

Important information about the nature of fracture can be obtained from microscopic examination of the fracture surface. This study is called fractography. Fractography is most commonly done using the scanning electron microscope (SEM). The large depth of focus and fact that the actual surface can be examined make the SEM an important tool for research and for failure analysis. On a microscopic scale the commonly observed fracture modes are cleavage, quasi-cleavage and dimple rupture. Cleavage fracture represents brittle fracture occurring along crystallographic planes. The characteristics feature of cleavage fracture is flat facets which generally are about the size of the ferrite grain. Usually, the flat facets exhibit river making. Quasi-cleavage fracture is related but distinct to cleavage fracture. It is observed chiefly in low-temperature fracture of quenched and tempered steel. Quasi-cleavage fractures often exhibit dimples and tear ridges around the periphery of the facets [49]. Dimples rupture is characterized by cup-like depressions that may be equiaxial, parabolic or elliptical depending on the stress state. This type of fracture denotes a ductile fracture. Microvoids are initiated at second phase particles, the voids grow and eventually the ligaments between the microvoids fracture.

The austenitic microstructure of AISI 316L steel in the as-received state was formed of fine grains with twins that corresponded to the pre-deformation of the material during its processing by cold forming. Twinning is generally observed as a deformation mechanism that is activated at high strain rates.

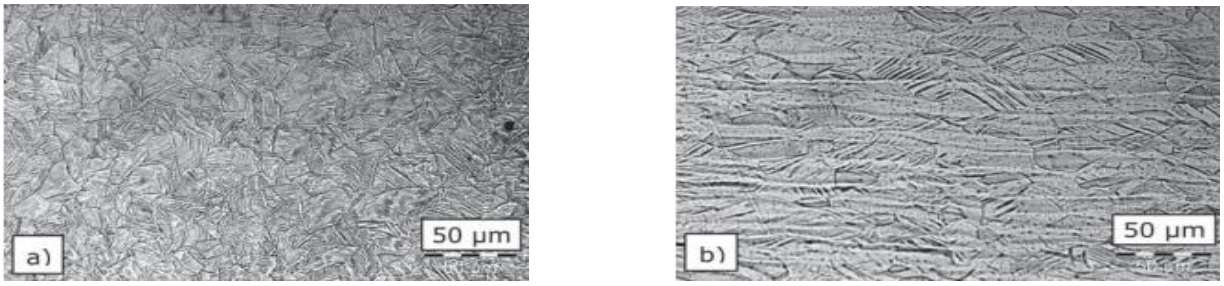

Fig 2.18*: Fine-grained microstructure of austenitic 316L in as-received state: a) transversal and b) longitudinal sections.*

2.7 POST RATCHETING BEHAVIOUR OF SOME MATERIALS

Initially ratcheting research has started on the macroscopic experimentation and constitutive modelling to simulate ratcheting behaviour. Conversely, the majority of the constitutive models are phenomenological in nature and build up entirely based on the macroscopic experimental observation only [52]. As a consequence, constitutive models with many material parameters have been developed but these models are not user-friendly. Therefore its use is limited in engineering application.

Kang et al. [38] have investigated the uniaxial ratcheting behaviour of ordinary 20 carbon steel (0.19% C, 0.22% Si, 0.46% Mn) (polycrystalline body-centered cubic (BCC) metal) by macroscopic and microscopic observations at ambient temperature. They have noticed the development of dislocation patterns from some low density modes (i.e., dislocation lines and networks) to high density modes (i.e., dislocation tangles, walls and cells) with number of cycles during LCF and ratcheting. The sub-grains are created by the re-arrangement of dislocations after a certain number of cycles in ratcheting [52].

Kang et al. and Dong et al. have examined the microstructural evolution during uniaxial and multiaxial ratcheting of 316 L stainless steel. The 316 L stainless steel has face centered cubic (FCC) crystal structure and also has low stacking fault energy (SFE, 15 mJ/m^2). For 316 L stainless steel, the progression of dislocation patterns is also similar as observed in 20 carbon steel during uniaxial and multiaxial ratcheting (i.e., dislocation arrangement alters progressively from the low density patterns to high density patterns). However due to the low stacking fault energy of 316 L stainless steel, the cross slip is not activated and dislocation cell is the stable dislocation arrangement for both the case of uniaxial and multiaxial ratcheting. On the other hand, for BCC 20 carbon steel sub-grain is the stable dislocation pattern during the ratcheting since the dislocation cross-slip is readily achievable in the BCC crystals. The comparatively higher ratcheting strain accumulation rates in BCC 20 carbon steel during uniaxial and multiaxial ratcheting at the stage II are normally caused by the dislocation re-arrangement during the development of sub-grain and activation of dislocation slip within the sub-grain [52].

Kang et al. [38] have investigated the uniaxial ratcheting response of Ti–6Al–4 V alloy with two phases (i.e., primary α phase with hexagonal close packed (HCP), and secondary β phase with BCC

crystal structures) at room temperature. They have noticed the progression of dislocation arrangement and formation of deformation/mechanical twin during uniaxial ratcheting. **The dislocation density and the number of twins grow with number of cycles**. Neither the dislocation wall nor cell is found in their investigation. They have only observed the activity of planar dislocation evolution in association with development of discrete dislocation lines, dislocation nets and parallel lines. Authors have studied the micro-mechanism of ratcheting quantitatively for the for AISI316 L stainless steel. **They have observed that no ratcheting strain evolution (i.e., cyclic creep) takes place during the cyclic plastic deformation with planar slip activity.** The plastic deformation could be recovered completely during the cyclic plastic deformation with planar slip activity because of the smooth movement of dislocations. Conversely, accumulation of ratcheting strain takes place during cyclic plastic deformation with cross slip activity as the unrecoverability of slip may possible be due to the increased resistance of dislocation movement during the cross slip [18]. Paul et al. have used EBSD data of DP 780 steel to quantitatively measure differences between LCF and ratcheting test samples. The average mis-orientation maps for the LCF and ratcheting specimens are depicted in Fig. 27. Paul et al. [27] have reported that there is a significant difference in the local in-grain mis-orientations for LCF and ratcheting. **The local in-grain mis-orientation is higher in ratcheting in comparison with LCF specimen. This is consistent with the observation of dislocation sub-structure by other researchers.** The ferrite misorientation is larger compared to the average around the martensite islands. This is direct confirmation of strain localization at the ferrite/martensite interface in the ferrite.

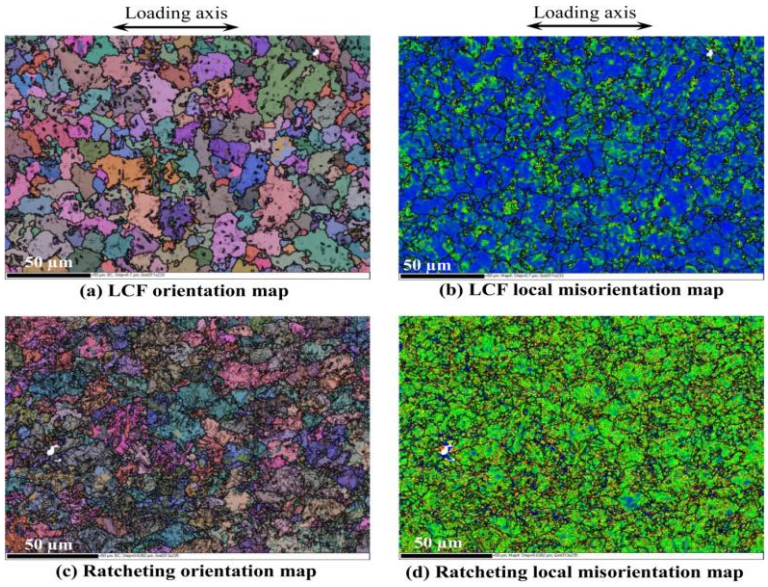

Fig 2.19: *EBSD orientation maps for two different test conditions, LCF (total strain amplitude of 0.5%), and Ratcheting (mean stress of 150 MPa and stress amplitude of 550 MPa). All Euler orientation maps are shown on the left with grain boundaries >10° shown in bold black lines, and grain boundaries between 3° and 10° shown in fine black lines. Local misorientation maps shown to same scale with blue showing low local misorientation, and yellow/green showing high local misorientation. Local misorientations shown with 5° cutoff. Mapping step size is 0.6 µm [27].*

CHAPTER-3

MATERIALS AND EXPERIMENTS

3.1 INTRODUCTION

The objective of the present thesis is to explore the ratcheting behavior of AISI 316L stainless steel. The study of tensile behavior at two different strain rates is also done in this investigation. There are many reasons for failure of engineering components during service. Among these, fatigue failure is one of the major concerns in case of cyclically loaded components. Fatigue behavior of materials is commonly studied under completely reversed cyclic stressing or straining. Because of such symmetric cyclic loading failure occurs without any gross plastic deformation and the fatigue life depends upon the imposed stress or strain amplitudes. But, during asymmetric cyclic stressing, i.e., cyclic loading with non-zero mean stress, along with fatigue damage cycle-by-cycle inelastic strain is accumulated in the specimen and final failure occurs on accumulation of certain amount of inelastic deformation. Such accumulation of inelastic strain during asymmetric cyclic stressing is known as "ratcheting deformation." The damage occurring due to ratcheting deformation deteriorates the cyclic life of specimens and components as compared to what happens in case of symmetric cyclic loading. It is, therefore, essential to understand the ratcheting behavior of different materials for safety and structural integrity purpose of cyclically loaded components.

The effect of stress parameters on ratcheting life or ratcheting strain rate evolution can be investigated in two different ways: i) using different combinations of mean stress and stress amplitude and ii) using different stress ratios at constant maximum or minimum stress level. It is well reported in literature that ratcheting strain evolution increases with increase in mean stress for a variety of materials having different hardening/ softening characteristics [17-19]. The mean stress and stress amplitude dependent asymmetric cyclic plastic behavior, mainly ratcheting-fatigue life, ratcheting strain and ratcheting strain rate have been studied by researchers over a variety of materials like: IF steel [20], SA 333 Gr. C-Mn Steel [21], SA 333 Steel [22], SS 304 Stainless Steel [23], Inconel 718 [19] and Cu alloy [24]. The three stages of ratcheting rate evolution have been studied by some of the above researchers [20, 22] and the variation has been looked into with respect to the mean stress and stress amplitude.

The details of the ratcheting test procedures are also presented in the chapter.

3.2 MAT ERIAL

The material as received for investigation is AISI 316L stainless steel. It has low carbon content. The chemical composition of the material is given in **Table 3.1**.

Table 3.1 Chemical Composition of 316L Plate

Elements	C	Mn	Si	S	P	Ni	Cr	Mo	Cu	N	Ti
Weight Percent (%)	0.025	1.72	0.367	0.0025	0.027	10.10	16.74	2.01	0.388	0.035	0.0028

3.3 MICROSTRUCTURE

Optical microscopy through Leica optical microscope (LEICA DM 2700M) fitted with a digital camera (LEICA DMC 4500) is done to reveal the microstructure of as-received 316L stainless steel plate. Sample preparation is a vital part of optical microscopy which consists of cutting of the sample, polishing and etching respectively. Polishing is done until scratch free, smooth mirror like surface is obtained and then etching is done. Etching is needed to reveal the microstructure of the specimen by etching contrast. Etchant used to reveal the microstructure is a solution of HCL and HNO_3 in the ratio 2:1 respectively.

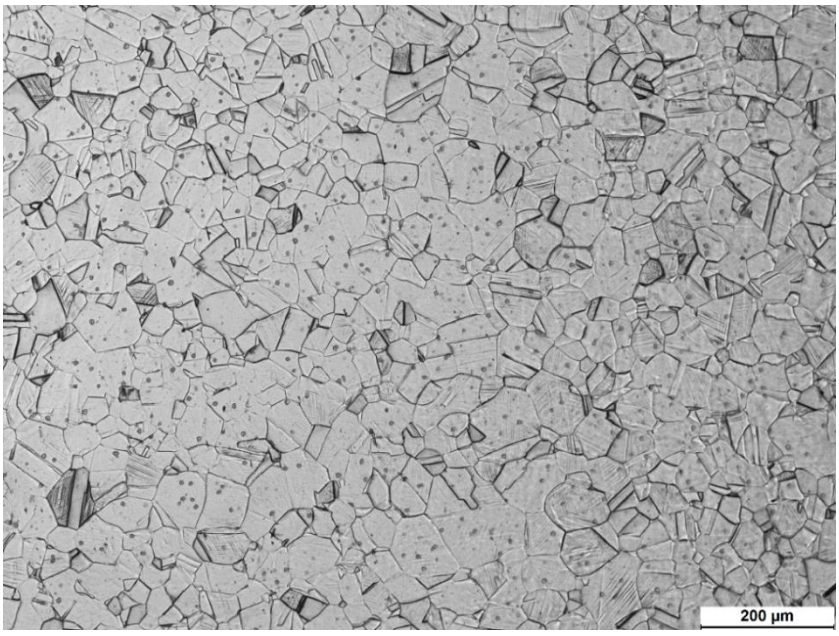

Fig 3.1: *Microstructure of 316L stainless steel*

Figure 3.1 shows the microstructure (OM) of 316L stainless steel. Optical microscopy reveals that the microstructure consists of polygonal shaped grains of austenite with some annealing twins interspersed in some grains.

3.4 FABRICATION OF TENSILE AND RATCHETING SPECIMEN

The specimen geometry used for tensile test and ratcheting test is shown in **Figure 3.2 and Figure 3.3**. The specimens have been fabricated from as-received condition 316L stainless steel plate (Thickness 20 mm) for rolling direction. All the tensile specimens were fabricated as per ASTM E8/E8M -2009 and ratcheting specimens were fabricated as per ASTM E606-92 (Reapproved 1998).

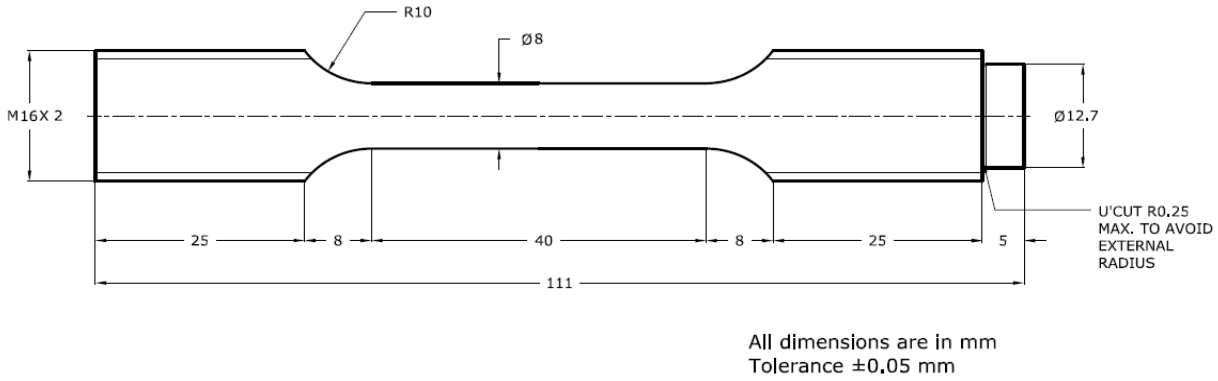

Fig 3.2: *Specimen geometry used for Tension Tests*

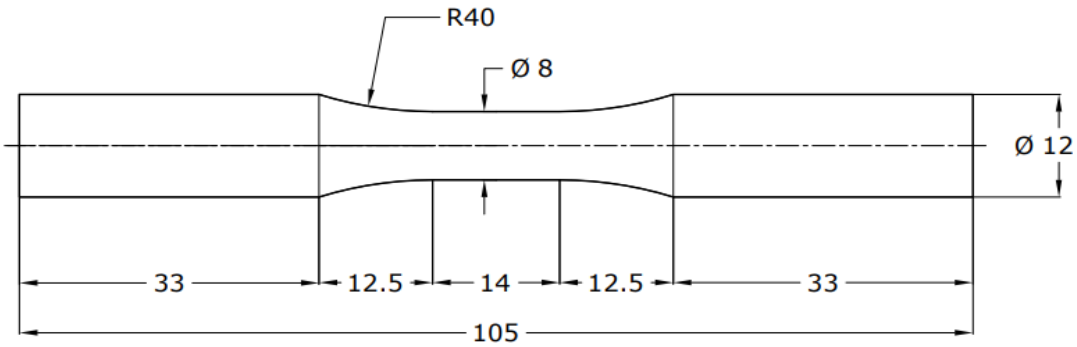

Fig 3.3: *Specimen geometry used for ratcheting tests*

3.5 TENSILE TEST

Tensile tests have been done in a computer controlled servo-electric universal testing machine, Instron 8862 (Instron, High Wycombe, U.K.) of ± 100 KN load capacity at room temperature [~300K (27 deg C)]. The tensile tests have been done at a strain rate of 10^{-3} and $3*10^{-3}$ sec^{-1} for rolling direction under strain control mode. An extensometer of 25 mm gauge with full range capacity of +100% to -10% has been used to control the tests and for strain measurement purpose.

3.6 RATCHETING TEST

All the ratcheting experiments were carried out at room temperature using a 100kN servo-electric testing system (Instron-8862) supported by Wave Matrix software. The system was attached to a computer to control the tests as well as for data acquisition. All tests were conducted in strain control mode till fracture using triangular waveform as per ASTM E 606 at a constant stress rate of 200 MPa/s. The schematic diagram for asymmetric stress control triangular waveform representing ratcheting test parameters is shown in **Figure 3.4**.

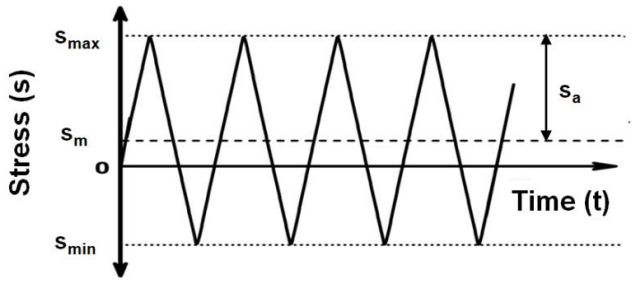

Fig 3.4: *Schematic representation of ratcheting test procedure (s_a is stress amplitude, s_m is mean stress, s_{max} is maximum stress and s_{min} is minimum stress).*

The test matrix used for asymmetric cyclic loading is shown in Table 3.2.

Table 3.2: Test matrix for ratcheting test

Mean Stress (MPa)	Stress Amplitude (MPa)	Maximum Stress (MPa)	Minimum Stress (MPa)	Stress Ratio (R)	Frequency (Hz)
20	380	400	-360	-0.90	0.13
40	360	400	-320	-0.80	0.14
60	340	400	-280	-0.70	0.15
80	320	400	-240	-0.60	0.16
100	300	400	-200	-0.50	0.17
120	280	400	-160	-0.40	0.18

The frequency (f) of cycling was calculated for each test by following equation

$$\boldsymbol{f = \frac{\dot{S}}{4 * S_a}} \qquad \text{Eq (3.1)}$$

Where, f = Frequency, $\boldsymbol{\dot{S}}$ = Stress rate and $\boldsymbol{S_a}$ = Stress amplitude

Extensometer of 12.5 mm gauge length and having ± 20% full capacity was kept attached to the specimen gauge section with help of O-ring to record the cyclic stress-strain data during test. The test was continued until complete failure of the specimens.

3.7 FRACTOGRAPHY

Fracture surfaces of 316L stainless steel specimens failed under asymmetric stress cyclic loading were carefully preserved and finally cleaned in an ultrasonic cleaner using acetone bath. The clean fracture surfaces of specimens were examined in a Scanning Electron Microscope (SEM), HITACHI SU 3800 under secondary electron imaging mode using an operative voltage of 20kV and working distance of 10.0±2.0 mm.

3.8 XRD ANALYSIS

Ratcheting specimen of 1 mm thickness is cut from the fractured surface and XRD analysis was done on Rigaku Ultima-III to examine the phases present in post ratcheting specimens. The presence of new phase was examined with the help of X-ray diffraction patterns.

CHAPTER-4

RESULTS AND DISCUSSIONS

4.1 INTRODUCTION

Tensile properties are important parameters to understand the general behavior of a material. Tensile behavior of AISI 316L austenitic stainless steel has been presented and discussed in **section 4.2**. Also, the ratcheting characteristics have been studied through a number of experiments and results are presented in **Table 4.3** of **section 4.3**. Cyclic plasticity and hardening-softening behavior during cyclic loading are important in the ratcheting deformation of 316L stainless steel. Fractography is also discussed in **section 4.3.**

4.2 TENSILE TEST

4.2.1 Engineering stress-strain behaviour of ASS 316L

Tensile specimens have been used to investigate tensile properties of the material at two different strain rates. Engineering stress-strain curve is shown in Figure **4.1** and the related properties in Table **4.1**.

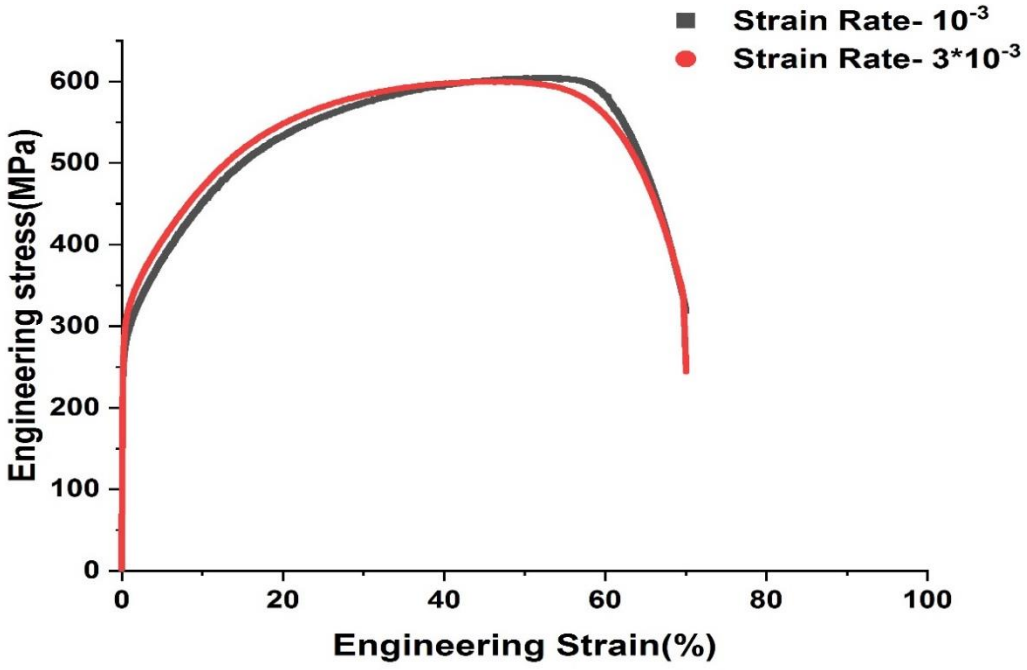

Fig 4.1: *Engineering stress-strain curve for 316L stainless steel*

Table 4. 1: Results of tension tests of specimens at different strain rates

Sl.No	Strain Rate (sec^{-1})	σ_{yt} (MPa)	σ_{uts} (MPa)	ε_u (%)	ε_t (%)	*K (MPa)*	*n*
1	0.001	264	604	50.1	60.4	1119	0.316
2	0.003	293	600	46	70.3	1094	0.287

4.2.2 True stress-strain behaviour of ASS 316L

The true stress (σ) vs. true strain (ε) curve of the investigated material is presented in **Figure 4.2**. The corresponding values of strain hardening exponent *n* and strength coefficient *K* were calculated using Hollomon's equation $\boldsymbol{\sigma = K\varepsilon_p^n}$. The obtained results are plotted as true stress vs true strain in the plastic domain which results into curves. The values of *n* were estimated by fitting power law curve and taking its exponent and *K* as the coefficient of the equation.

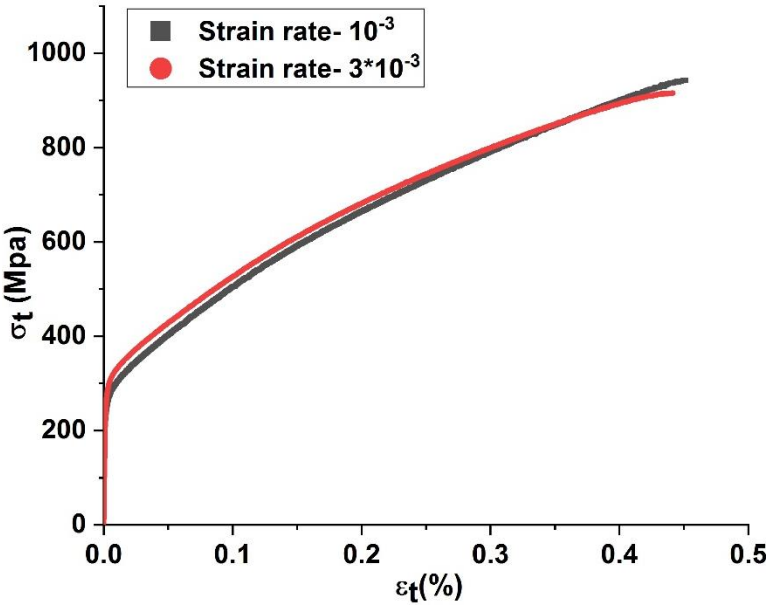

Fig 4.2: *True Stress vs True Strain curve for AISI 316L*

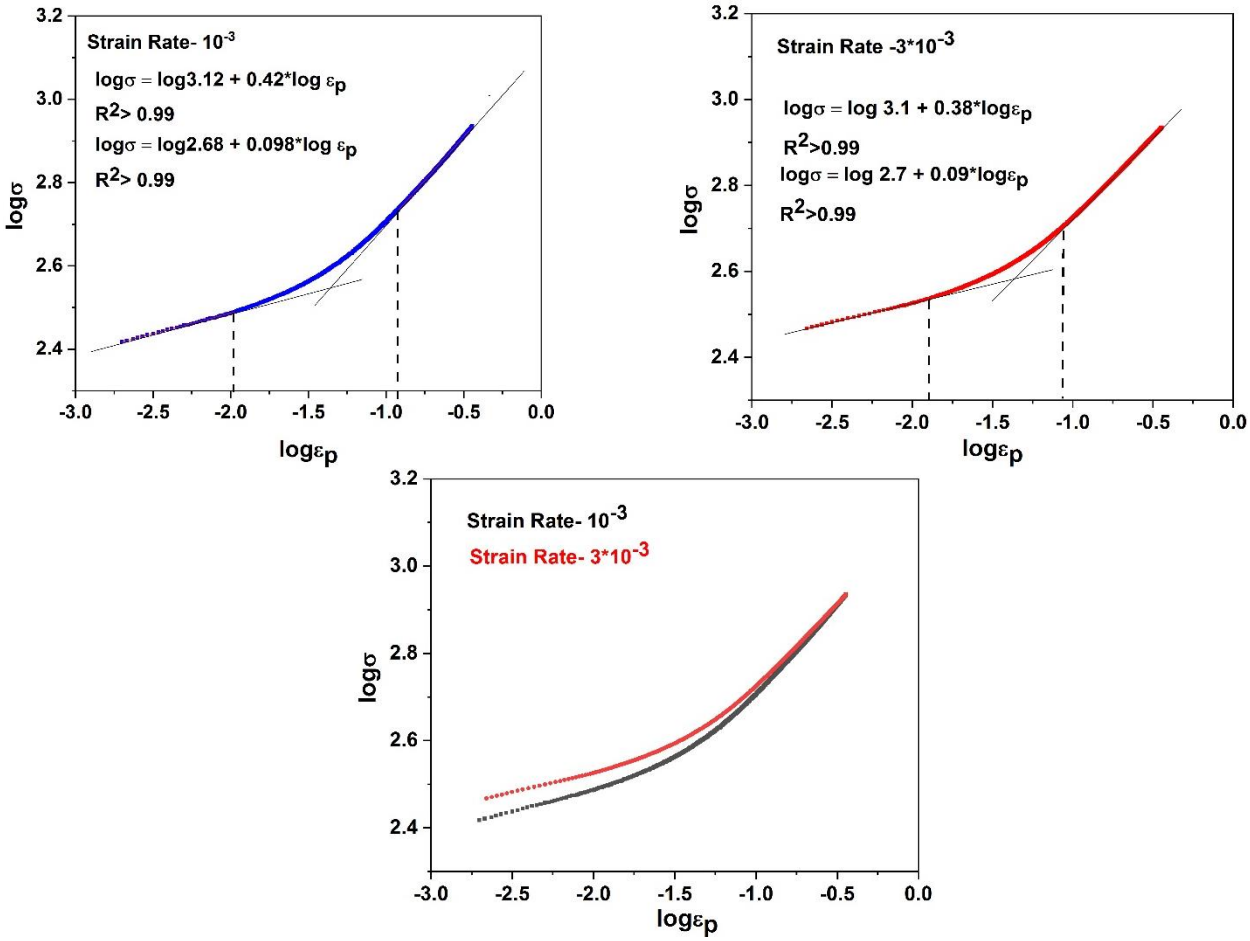

***Fig 4.3**: Hollomon analysis at different strain rates*

True stress (σ) - true plastic strain (ε_p) plot on double logarithmic scale should yield a straight line; the slope of which is known as strain hardening exponent (n). But it is observed that ln(σ) vs ln(ε_p) plot does not follow a single straight line relationship as shown in Figure 4.3. It suggests that plastic deformation of investigated annealed AISI 316L stainless steel do not follow a single mechanism, Instead of a single straight line, two different straight lines i.e. two different hardening stages (Stage-I and Stage-II) are observed in case of 316L as shown in Figure 4.3. It is observed that strain hardening exponent in Stage-I is lower compared to the Stage-II deformation. The transition of plastic deformation i.e., from Stage-I to Stage-II does not occur sharply. Rather there is a transition region and the deformation mechanism slowly changes from Stage-I to Stage-II. Here Stage-I is from -2.75 to -2 and stage-II is from -1.5 to -0.5 on the X-axis.

4.2.3 Fractographic analysis of tension test specimen

To observe the fracture surface of the failed specimen at the strain rate of 0.001 per sec, SEM images have been captured. Fig 4.4(a) shows the complete view of the fracture surface of the specimen. Fig 4.4(b) shows the fracture morphology of the specimen observed under scanning electron microscopy (SEM).

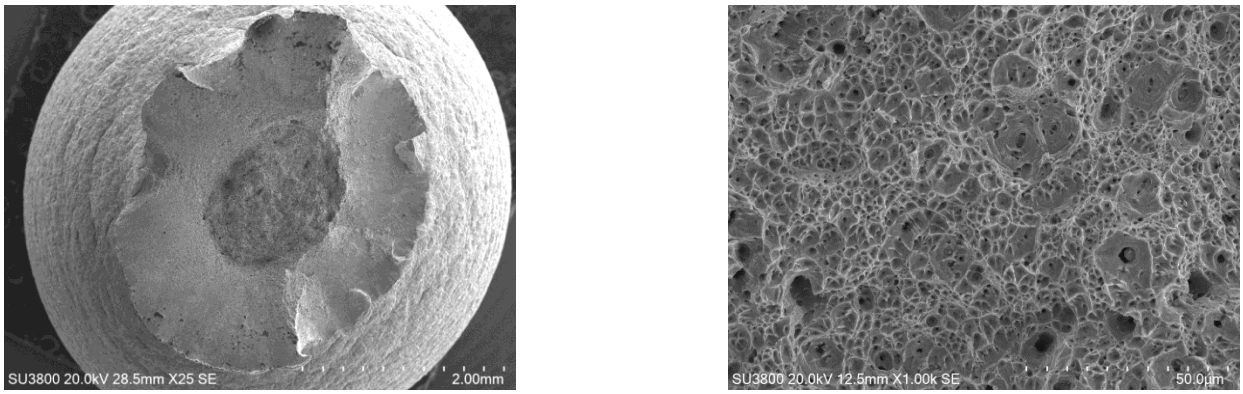

Fig 4.4*(a) SEM Image of fracture surface under tension test (b) SEM image of the same surface showing microvoids nucleation.*

Figure 4.4(b) clearly shows the micro voids nucleation that ultimately leads to fracture. The cup and cone type ductile fracture is clearly visible in this figure. The tensile fracture morphologies reveal that void nucleation, void growth and their coalescence constituted the fracture of the specimens.

4.3 RATCHETING BEHAVIOUR OF ASS 316L

The non-close stress-strain hysteresis loops developed during stress-controlled asymmetric cyclic loading have been presented in Figure 4.5 as a representative schematic diagram. It can be easily understood from figure that hysteresis loops shift in the direction of mean stress as the cycle goes on. Accordingly peak strains (both maximum and minimum) in each cycle increases from the respective values of the preceding cycle. The true ratcheting strain (ε_r) in every cycle has been calculated according to the following relationship:

$$\boldsymbol{\varepsilon_r = \frac{1}{2}(\varepsilon_{max} + \varepsilon_{min})} \qquad \textbf{(4.1)}$$

Where, ε_{max} and ε_{min} represent maximum and minimum axial true strain values in every cycle in the tensile and compressive directions respectively.

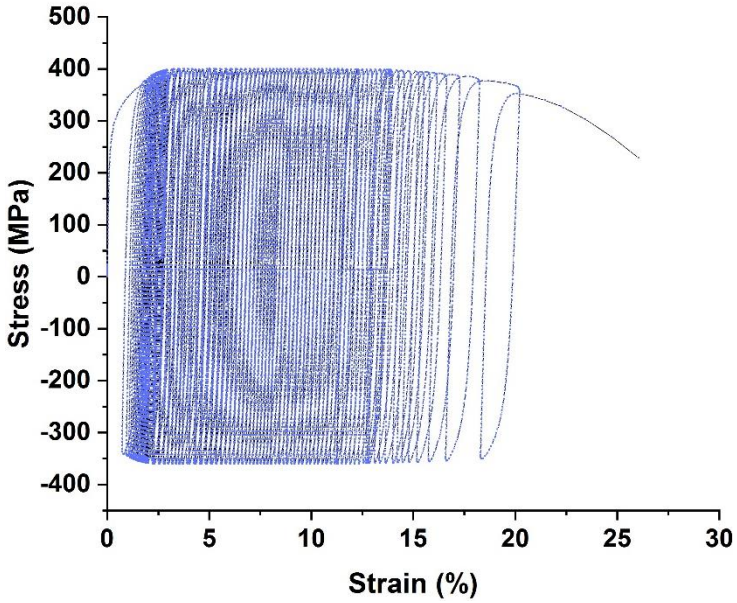

Fig 4.5: *Representative diagram of non-closed hysteresis loop shifting along strain axis*

Table 4. 2: Results of Ratcheting tests of specimens

Sl.No	σ_{max} (MPa)	σ_{min} (MPa)	σ_{mean} (MPa)	σ_{amp} (MPa)	*R-ratio*	*Number of cycles*	*Max. Ratcheting strain (%)*
1	400	-360	20	380	-0.9	969	20.089
2	400	-320	40	360	-0.8	1578	25.5278
3	400	-280	60	340	-0.7	2849	14.1589
4	400	-240	80	320	-0.6	5707	12.42708
5	400	-200	100	300	-0.5	14141	22.21325
6	400	-120	120	260	-0.4	22548	9.3414

4.3.1 Ratcheting strain curves

It can be observed from Figure 4.6 that accumulation of ratcheting strain occurs in three different stages. In the first stage ratcheting strain evolution increases rapidly irrespective of stress

combinations. This is followed by a steady state; finally ratcheting strain accumulation occurs very rapidly due to increase of true stress caused by large decrease of specimen cross-sectional area.

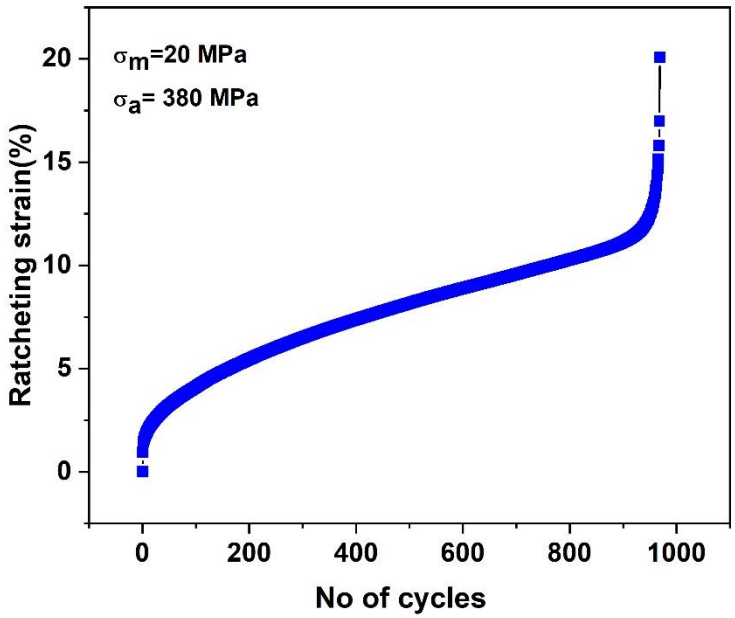

Fig 4.6: *Ratcheting strain vs no of cycles*

Variation of ratcheting strain, for different values of mean stress and amplitude stress at a constant maximum stress, with number of cycles is shown in Fig 4.7. It can be clearly seen from the fig 4.6 that ratcheting strain increases monotonically for any combination of mean stress and amplitude stress.

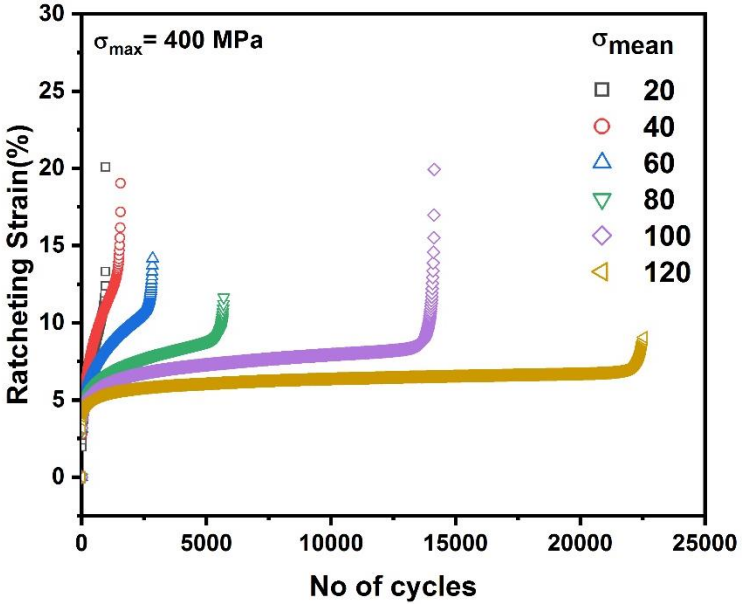

Fig 4.7: *Ratcheting strain vs number of cycles for different values of mean stress at constant maximum stress for 400 MPa.*

But specifically it can be seen that for lower value of mean stress and constant maximum stress ratcheting strain (%) is more as compared to higher values of mean stress.

Generally, it is observed that during asymmetric cyclic loading, either at constant mean stress or at constant stress amplitude, elongation of the specimen occurs without any plastic shakedown effect due to accumulation of inelastic strain in the direction of mean stress.

In these cases after accumulation of about 5-10% ratcheting strain no further strain is accumulated with progression of cyclic loading and thus tests were terminated. More specifically for mean stress of 120 MPa ratcheting strain accumulation is 5 %, for 100MPa mean stress it is about 7.5% and so on. Therefore it can be said that at constant value of maximum stress when the mean stress is increased ratcheting strain accumulation is reduced.

4.3.2 Failure number of cycles vs stress ratio

Stress ratio is the ratio of minimum stress and maximum stress. The plot of N_f vs stress ratio is shown in the fig 4.8, where N_f is the number of cycle at which the specimen failed.

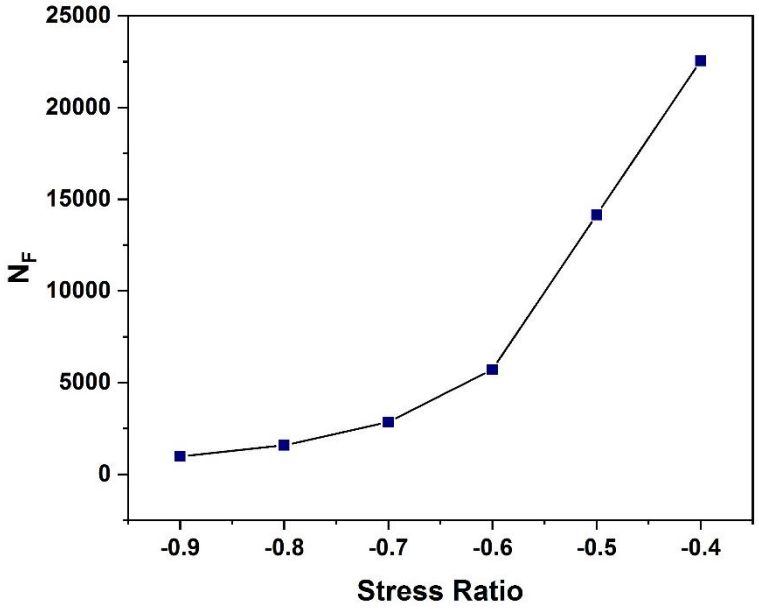

Fig 4.8: *N_F vs Stress ratio*

As the value of stress ratio is increased number of cycles to failure is also increased. Therefore it takes less number of cycles to fail for a specimen with higher value of mean stress or lower value of amplitude stress when maximum stress is kept constant.

It can also be deduced from the graph that when the specimens stress ratio is decreased from 0.9 to 0.6 there is slight increase in number of failure cycle but when the stress ratio has gone below 0.6 there is a sudden rise in the number of failure cycles.

4.3.3 Ratcheting strain Rate

As the variation of ratcheting strain with number of cycles of failures is already analyzed in section 4.3.2, it is very obvious to ask a question that what will be the variation trend for ratcheting strain rate with the number of cycles of failure. To understand the variation trend the graphical representation of the same is observed in fig.4.9. Here in the figure shown below, it can be seen that the general trend is the decrease in ratcheting strain rate with the increase in number of failure cycles keeping the maximum stress constant while varying the combination of mean stress and amplitude stress. But to be specific initially ratcheting strain rate was falling rapidly for a material with 20 MPa mean stress then for 40 MPa and so on. This trend is visible till 15 to 20 cycles after that the specimen having more value of mean stress has shown more rapid fall in value of ratcheting strain rate.

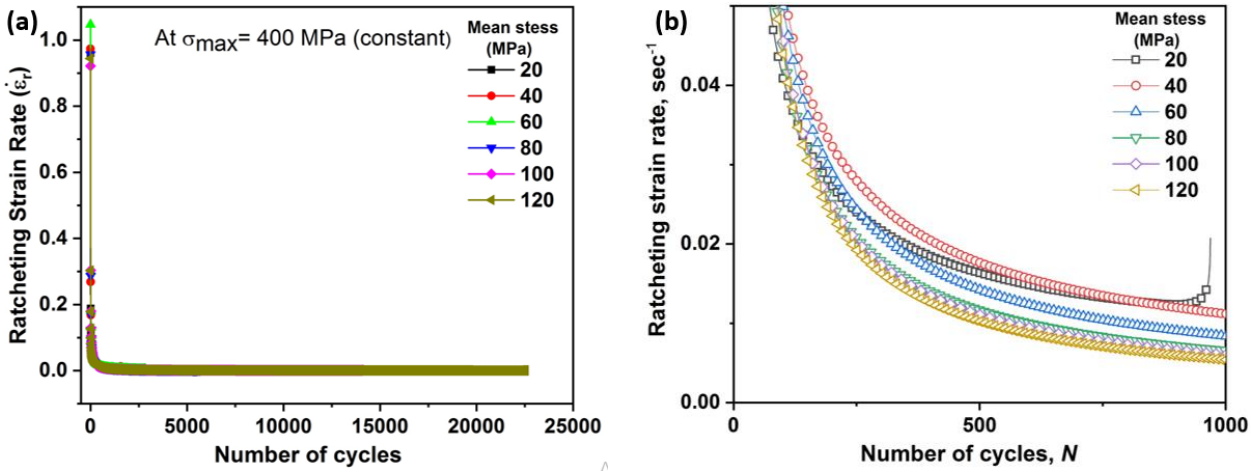

Fig 4.9: *Ratcheting strain rate vs Number of cycles*

Obviously the rise of mean stress results in the fast enhancement of the uniaxial ratcheting strain accumulation. Ultimately decrease in ratcheting life can be observed. Moreover, both the increase of ratcheting strain accumulation rate and reduction of ratcheting life are few folds when the mean stress is moved up from 20 to 120MPa.

4.3.4 Stress-Strain Hysteresis loop variations

Cyclic stress-strain behavior in materials is characterized by hysteresis loops in plots of stress versus strain. These loops occur because energy is dissipated in the material, causing a lag in the response (strain) of the material to a forcing function (stress) during; cyclic deformation.

Stress-strain hysteresis behavior in metals, as depicted by the size and shape of the hysteresis loop, is dependent on the micro-mechanisms which dissipate energy during cyclic deformation. The ability of materials to dispel energy by internal adjustments is referred to as damping. Specific damping energy is the amount of energy dissipated in a unit volume of material per cycle and is simply the area inside the stress-strain hysteresis loop. Although the size of the hysteresis loop is a measure of the energy absorbed per cycle, the shape of the loop, which is represented by the terms

in the rheological epicycle formulation, may be significant in determining the mechanisms which operate during cyclic deformation and the changes which occur in hysteresis behavior. Cyclic loading produces changes in material structure and properties which depend on the material and test conditions. The most obvious results of cycling are the cyclic softening or hardening which are detected by a change in the dependent variable (stress or strain) during testing.

Cyclic softening of cold worked metals is revealed by a decrease in stress necessary to produce a given strain in strain-controlled cyclic tests or an increase in strain for a given stress in stress-controlled tests. The way in which a material cyclically softens depends mainly on the extent of initial deformation, the magnitude of the cyclic stress or strain limits, and the number of cycles imposed. Observation of changes which occur in hysteresis loop size and shape has been fruitful in studying this phenomenon.

Manifestation of cyclic hardening exists in the increased stress necessary to attain a given strain in strain-controlled cycling and the reduction of strain for a given stress in stress-controlled cycling. Most annealed metals cyclically harden at a rate which increases during early cycles and subsequently decreases, indicating that plastic strain in cyclic deformation may be non-hardening.

Changes in hysteresis loop size and shape as a function of the testing and material variables and as a result of mechanisms operative during cycling offer an interesting and valuable way of viewing the cyclic behavior of materials. The monotonic stress-strain curve is not sufficient to predict mechanical behavior during cyclic loading. In addition, hysteresis loops are free of discontinuities and other geometric irregularities which are often present in monotonic stress-strain curves, making them more amenable to mathematical analysis.

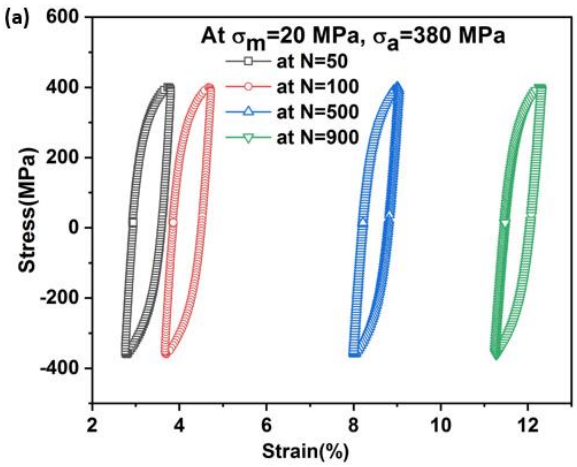

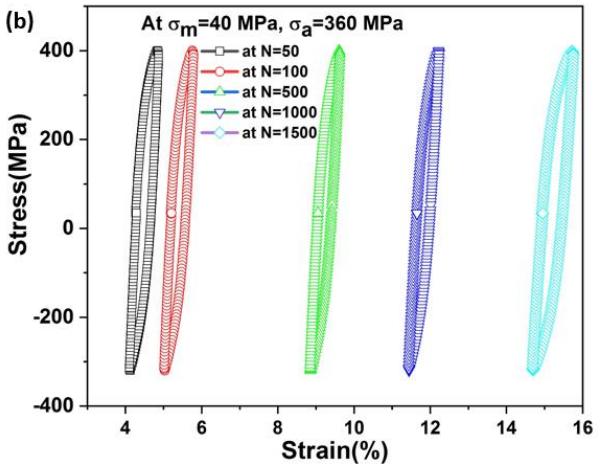

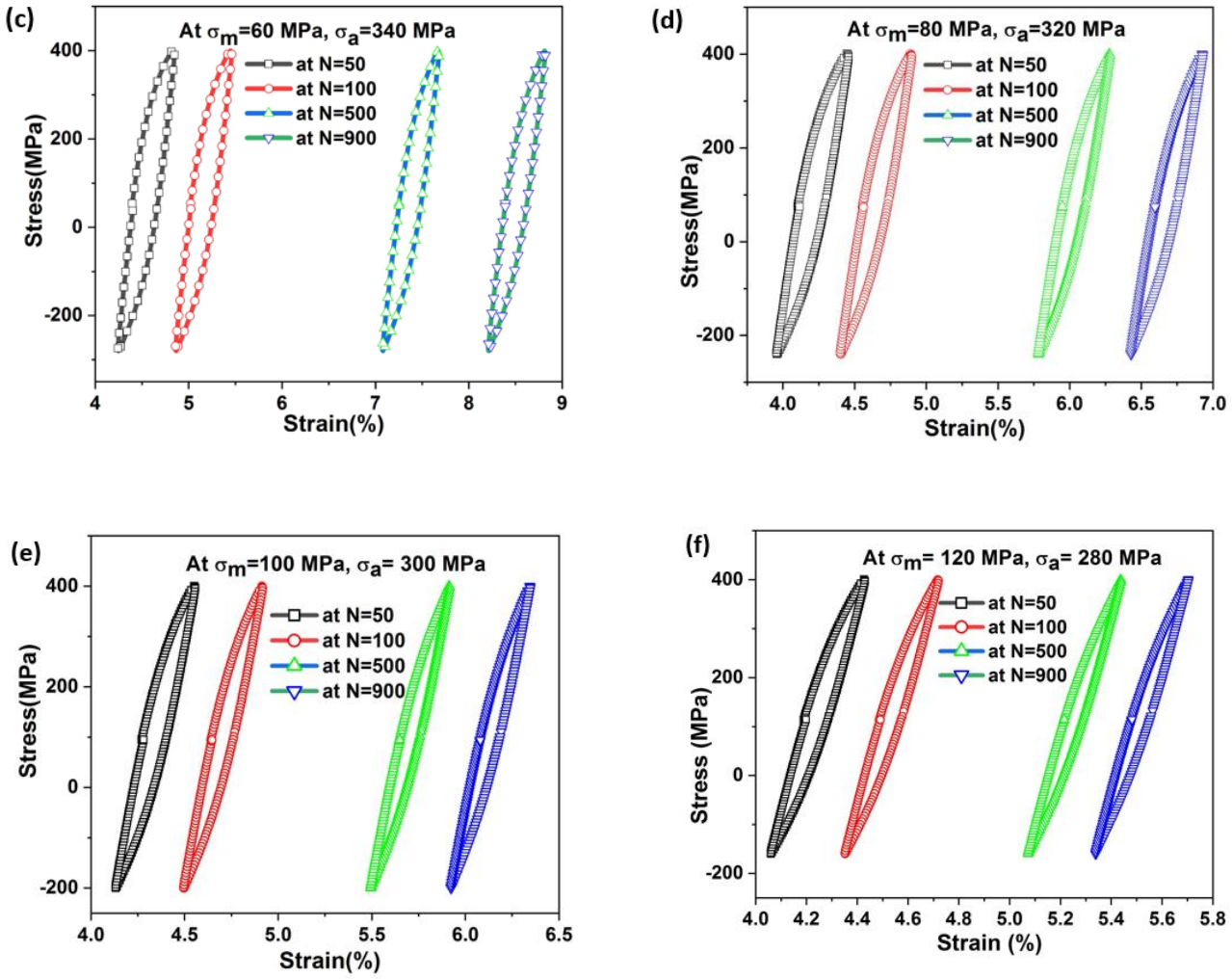

Fig 4.10. *Stress-strain hysteresis loop at (a)σ_m=20 MPa, σ_a=380 MPa, (b) σ_m= 40 MPa, σ_a=360 MPa, (c) σ_m= 60 MPa, σ_a=340 MPa, (d) σ_m= 80 MPa, σ_a=320 MPa, (e) σ_m= 100 MPa, σ_a=300 MPa and (f) σ_m= 120 MPa, σ_a=280 MPa*

Stress-strain hysteresis loop is plotted for four different value of cycle (N) i.e., N=50,100,500 and 900 for combination of 20MPa mean stress and 380MPa stress amplitude at constant maximum stress in Fig 4.10(a). Similarly others plots of stress strain are also plotted for different combinations of mean stress and amplitude stress or different value of cycle number. These plots are shown as Fig 4.10 (a-f).

For different setoff values of mean stress and stress amplitude at constant maximum stress it can be seen clearly that there is slight variations in the stress-strain curves at same value of cycle i.e., N=50,100,500 and 900 in most of the cases.

Stress-strain laws for materials in the amplitude independent category are essentially linear, containing stress, strain, and their time derivatives. The area of the hysteresis loop generated by dynamic loading is frequency dependent, the loop generally; being elliptical in shape.

It can be observed through different graphs that there is slight tilt or we can say that at the same value of stress, strain (%) has increased while increasing the mean stress. The orientation of hysteresis loop can be seen as somewhat turning on increasing the value of mean stress.

But overall it can be said that the strain accumulation is decreased when mean stress is increased or amplitude stress decreased keeping maximum stress constant. For example, for N=900 cycle at mean stress of 20MPa strain accumulation (%) is around 11%, at mean stress of 60MPa it is around 8-8.5%, for mean stress of 80MPa it is somewhat around 6.5%, for mean stress of 100MPa it is 6% and for mean stress of 120MPa it is again reduced to around 5.4%.

So it is very much clear that for same value of N and maximum stress, when mean stress is increased or amplitude stress is reduced strain accumulation is also reduced.

When the various hysteresis loop obtained from different combinations mean stress and amplitude stress are analysed, we found that the loop width is decreasing with increasing number of cycle. Also it tends to cause plastic shakedown. This trend is more or less applicable to all the different combinations of mean stress and amplitude stress.

The decrease in width of hysteresis loops also indicates that the cyclic hardening has increased with increasing number of cycles. Instead if hysteresis loops width has increased with increasing number of cycles without causing plastic shakedown then that would indicates toward cyclic-softening.

4.3.5 Strain Energy Density

For better understanding of strain energy density, first the strain energy should be known well.

When a force is applied to a solid, it deforms. The work done by the applied force is stored in the solid as potential energy. Mathematically, this energy is a balance of the work done due to external loads (such as body forces, surface tractions, point loads) and volume integral of the work done due to internal stresses. The latter is referred to as strain energy.

To normalize this property throughout the material, it is easiest to think of strain energy density, which is the strain energy per unit volume. Then, total strain energy comes from the integration of strain energy density over the volume of a body. Thus, we can express strain energy density in SI units of J/m3.

Strain energy density also shares the same unit with stresses: Pascal.

$$\frac{\boldsymbol{J}}{\boldsymbol{m^3}} = \frac{\boldsymbol{N * m}}{\boldsymbol{m^3}} = \frac{\boldsymbol{N}}{\boldsymbol{m^2}} = \boldsymbol{Pa}$$

Another definition for strain energy can be obtained from the stress-strain diagram shown below. For a uniaxial stress state, it can be defined as the area under the curve bounded between point (0,0) where no load is applied and (ε_x,σ_x) at which a normal stress is applied:

$$\boldsymbol{Strain\ Energy\ Density} = \int_0^{\varepsilon_x} \boldsymbol{\sigma_x\, d\varepsilon} \qquad \textbf{(4.2)}$$

Strain energy density is the amount of strain energy absorbed per unit volume of the object. It is also known as the amount of work required to cause deformation in a unit volume of the object. It is denoted by the symbol 'u' and it is equal to the area under the stress-strain curve.

Now for our experimentation, the plot of **strain energy density and no of cycles** is obtained for different combinations of mean stress and amplitude stress keeping maximum stress constant. The graphs can be seen below as fig 4.11:

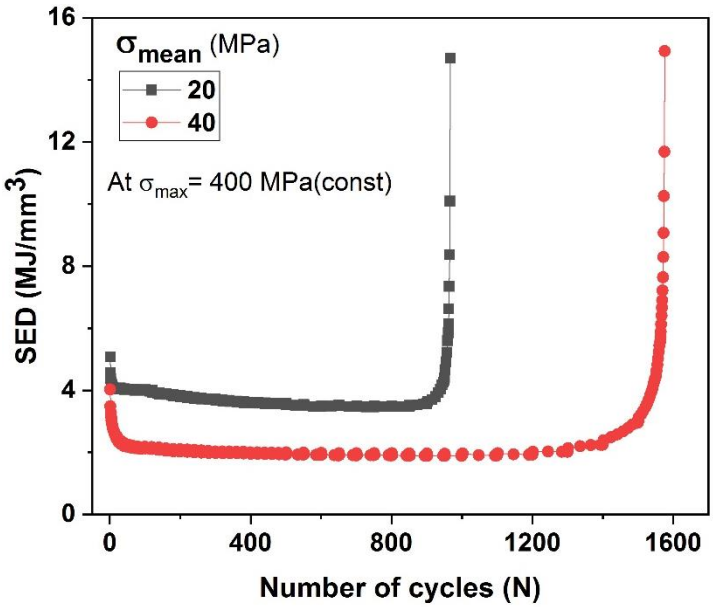

Fig 4.11: *Variation of Strain energy density with number of cycles (a) at mean stress 20MPa and stress amplitude 380MPa (b) at mean stress 40MPa and stress amplitude 360MPa*

Likewise it can be observed from these graphs that with the increase in mean stress or decrease in amplitude stress keeping maximum stress constant materials require more number of failure cycles for doing same amount of work against deformation.

To understand more precisely about the ratcheting behavior of 316L ASS let us see the variation in strain energy density with respect to mean stress for all the six combinations of experimental data. The figure 4.12 shows the variation of strain energy density (SED) with mean stress of 20,40,60,80,100 and 120MPa for three different values of cycle i.e., N=10,100 and 500.

It is obvious for any particular number of cycle that the strain energy density decreases with increase in mean stress. That can be verified easily with the above plot. It can also be deduced from the same graph that for a constant mean stress value while increasing the number of cycles Strain energy density is reduced.

Therefore it can be seen clearly from the graph that 316L specimen at constant mean stress always has less strain energy density with increasing number of failure cycles.

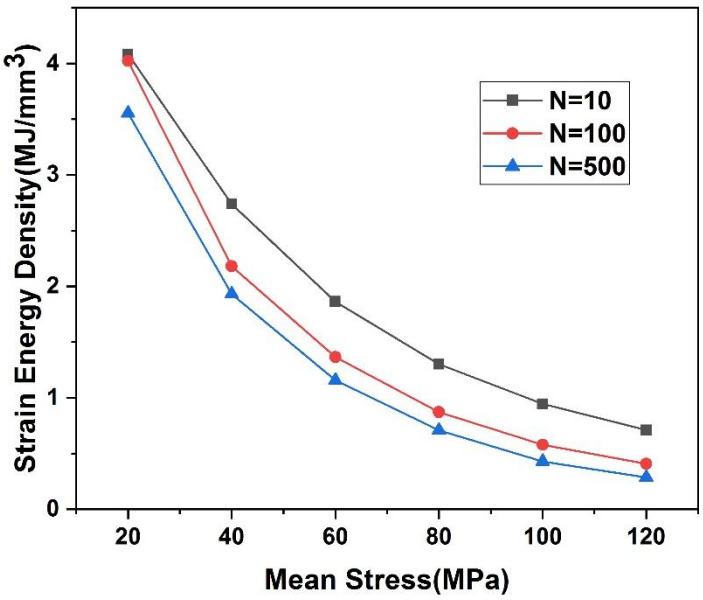

Fig 4.12: SED vs Mean stress

It has been discussed by many authors that with increasing magnitude of amplitude stress (at constant mean stress), $\boldsymbol{\varepsilon_{rf}}$ increases with attendant decrease in N_f. While it is observed that at constant amplitude stress, $\boldsymbol{\varepsilon_r}$ increases with attendant increase in N_f. The increase or decrease in fatigue life may be explained with the extent of damage occurring in each cycle. The extent of damage occurring in each cycle can be considered as proportional to the energy associated in a particular cycle, i.e. the area under the hysteresis loops. It is noted from the obtained results (Fig. 4.12) that the energy can increase or decrease depending on the type of loading.

It can be deduced from the plot that when mean stress increases at constant maximum stress, the energy associated with progressing cycles decreases. As a result, damage accumulation is slower and the specimen takes longer duration to fail, which means increase in N_f.

4.3.6 Fractography

Fracture surfaces of the fatigue tested specimens were studied using scanning electron microscope. For this investigation, 6 set of representative fatigue specimens which failed during cyclic loading were carefully cut and the fracture surface were examined. The fractograph observed shows striations marks which reveals fatigue fracture. The micro-void pattern shows that the fracture is of ductile nature. This indicates a ductile fracture with micro-void morphology, which is associated with the nucleation, growth and coalescence of micro-cavities. Figures 4.13(a, b) shows fracture morphology of specimen of 20 MPa mean stress, similarly 4.14(a, b) shows fracture morphology of specimen of 40 MPa mean stress. Likewise 4.15(a, b), 4.16(a, b), 4.17(a, b) and 4.18(a, b) shows fracture morphology of 60,80,100 and 120 MPa mean stress respectively under SEM.

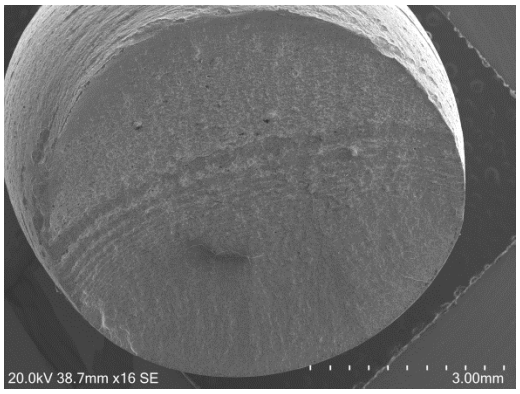

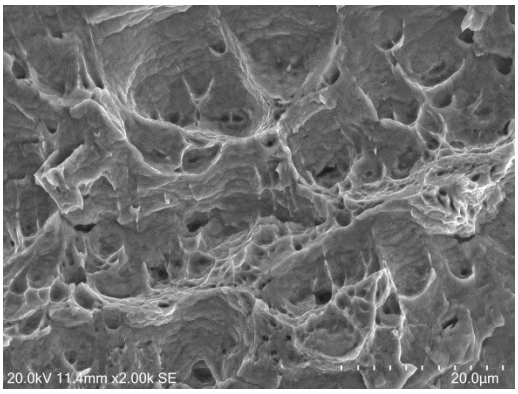

4.13*(a) SEM fracture morphology of specimen of 20 MPa mean stress (b) fracture morphology of the same showing micro-voids*

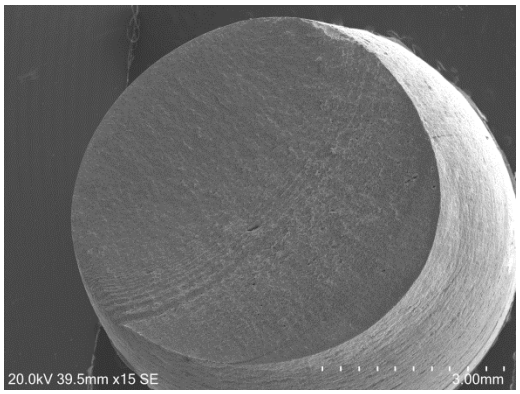

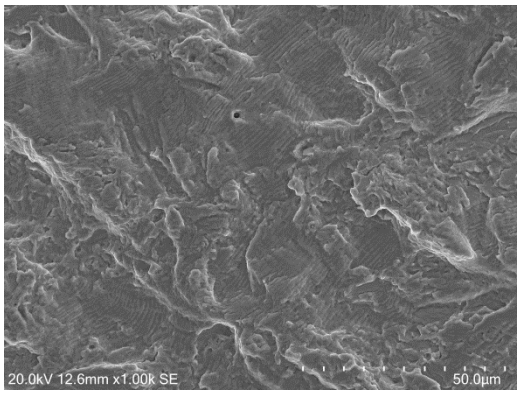

4.14*(a) SEM fracture morphology of specimen of 40 MPa mean stress (b) fracture morphology of the same showing micro-voids*

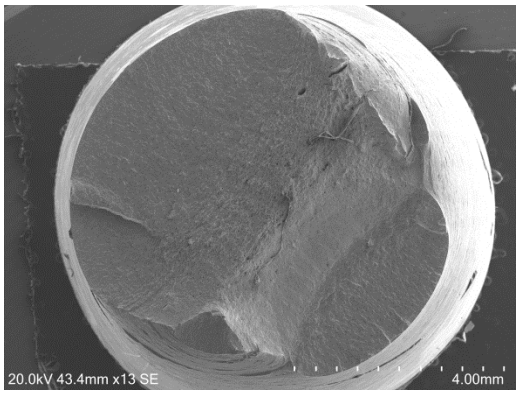

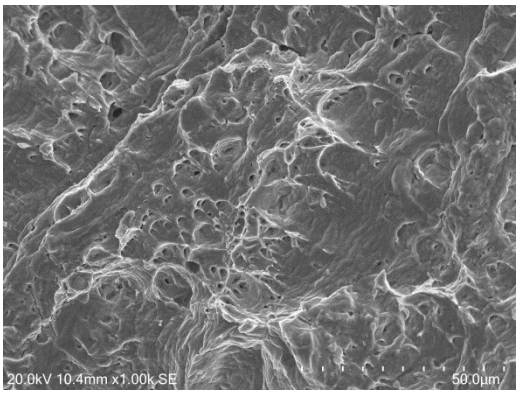

4.15*(a) SEM fracture morphology of specimen of 60 MPa mean stress (b) fracture morphology of the same showing micro-voids*

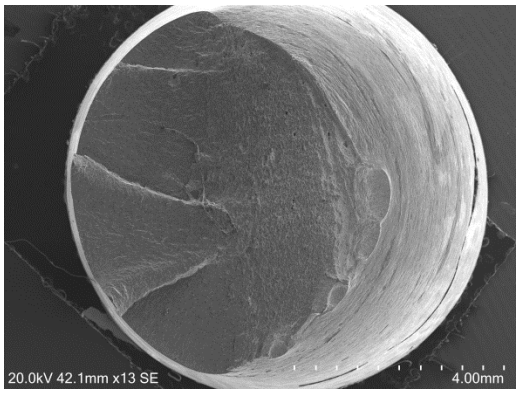

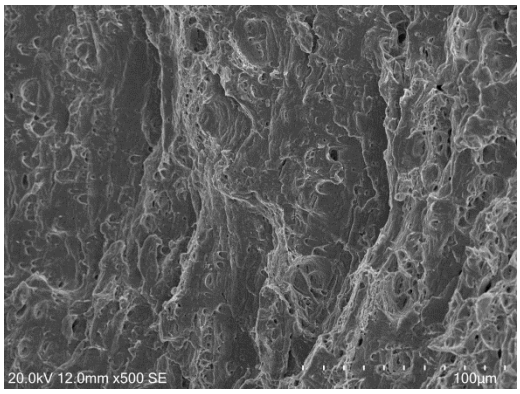

4.16*(a) SEM fracture morphology of specimen of 80 MPa mean stress (b) fracture morphology of the same showing micro-voids*

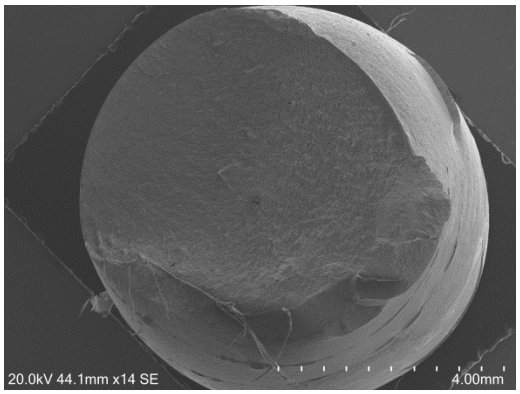

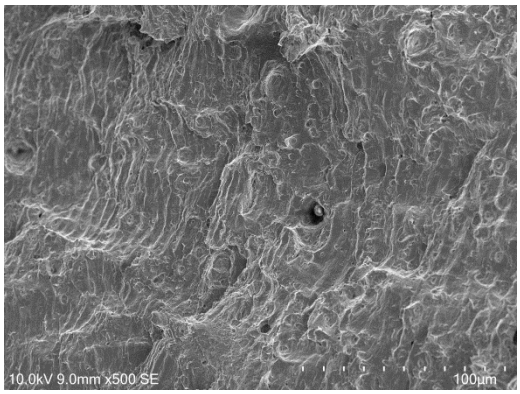

4.17*(a) SEM fracture morphology of specimen of 100 MPa mean stress (b) fracture morphology of the same showing micro-voids*

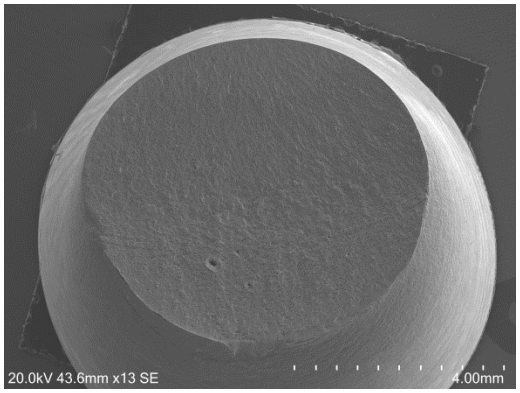

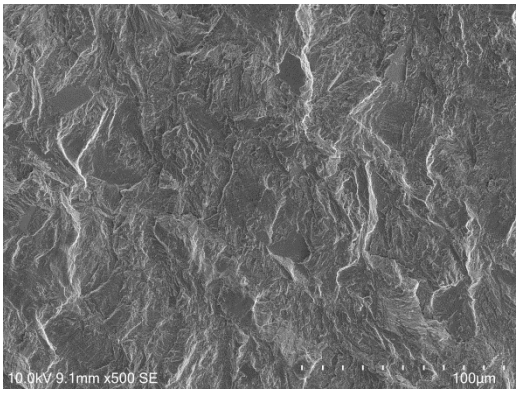

4.18*(a) SEM fracture morphology of specimen of 120 MPa mean stress (b) fracture morphology of the same showing micro-voids*

These images depict the possibility for damage accumulation during ratcheting could be through superimposition of micro-damages occurred by micro-void formation or micro-crack initiation. During the cyclic loading, micro-damage (cracks/voids) may occur in the substructure of the specimen, specifically in the interior of the dislocation cell/dislocation tangles or at the grain or phase boundaries. The micro-void/micro-crack generation may cause absorption of some energy, indicating higher damage and lower life. In case of specimens indicating higher N_f, micro-damage starts at a later period indicating longer life.

4.3.7 XRD Analysis of Ratcheting specimen

Comparative analysis has been done on 316L stainless steel between as received and deformed specimen by use of X-ray diffraction (XRD). The ratcheting tested specimen that undergone failure at 40 MPa mean stress and 360 MPa stress amplitude has been taken for X-ray diffraction (XRD) analysis. After deformation martensitic transformation in 316L stainless steel has been closely observed.

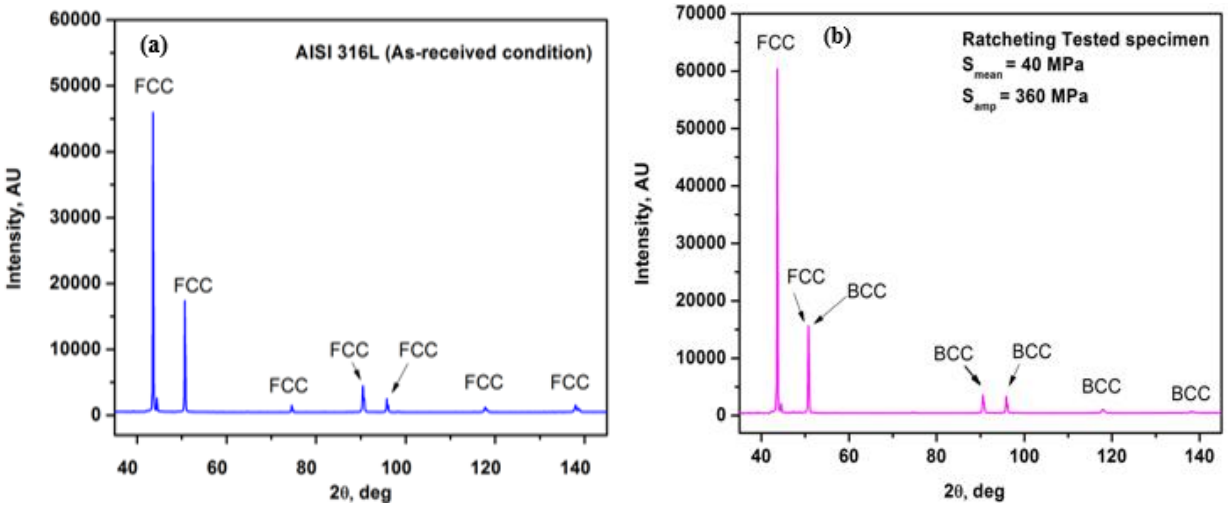

Figure 4.19. *(a) X-ray diffraction traces of AISI 316L stainless steel for as-received condition and (b) X-ray diffraction traces of deformed specimen (ratcheting test specimen)*

The crystallographic evolution can be observed after ratcheting test of an as-received specimen. In as-received specimen, only face centered cubic (fcc) crystal structure peaks can be seen clearly, but post testing, body centered cubic(bcc) crystal structure peaks can also be observed along with fcc crystal structure. This change can be attributed to the formation of the deformation induced martensite during testing [3].

CHAPTER-5

CONCLUSIONS AND FUTURE SCOPE

5.1 Conclusions

The present thesis is an attempt to characterize the ratcheting behaviour of ASS 316L at different combinations of mean stress and amplitude stress keeping maximum stress constant. The true stress controlled ratcheting test until complete failure of specimens were carried out at a stress rate of 200MPa/s at different mean stress keeping maximum stress constant. A triangular waveform was used for cyclic loading. The frequency of cycling was adjusted for each combinations of mean stress to maintain the nominal stress rate of 200MPa/s. An extensometer of full range capacity of -20 to +20% was properly kept attached to specimen gauge section with the help of o-ring for cycle-by-cycle monitoring of the specimen strains during stress cycling. More than 200 data points were collected for plotting stress-strain hysteresis loop. Test were controlled and data acquisition was done with the help of machine dedicated wavematrix fatigue testing software (Instron,UK).

This investigation leads to the following conclusions:

1. Ratcheting strain to failure accumulation linearly increases with increase of mean stress.

2. Ratcheting fatigue life exponentially increases with increase of mean stress. The hardening associated with increase of mean stress and lowering of Strain energy density per cycle increases the ratcheting fatigue life.

3. Rise of mean stress has an immense effect. It has fast enhancement of uniaxial ratcheting strain accumulation and decrease in fatigue life.

4. During engineering stress-control asymmetric cyclic loading accumulation of ratcheting strain occurs in three distinct stages irrespective of stress combinations.

5. The direction of ratcheting strain accumulation is identical with the mean stress direction in absence of pre-straining, complex multiaxial loading or other metallurgical factors.

6. Ratcheting life is higher for high UTS to Yield strength ratio.

7. True stress controlled ratcheting life increases more with lowering ratcheting strain accumulation compared to engineering stress controlled.

8. Reduction of plastic strain energy with increasing mean stress leads to improvement of ratcheting life.

9. The most detrimental effect in cyclic loading is the superimposition of two simultaneous damage processes, namely, progressive directional permanent strain accumulation and the fatigue damage due to continuous stress-strain hysteresis loop formation.

5.2 Scope of Future Work

Austenitic stainless steels are candidate materials for many engineering applications owing to their excellent strength, ductility, toughness even at low temperatures and non-magnetic nature. In heat-transfer pipelines of heavy water reactors of nuclear power plants, underground pipelines etc. the steel is potentially used, where components frequently encounter cyclic loading. However, during prolonged service at high temperature and with aggressive environments the steel suffers from grain boundary corrosion known as sensitization.

This thesis has been presented in connection with the investigation associated with ratcheting behavior of AISI 316L stainless steel. Ratcheting strain accumulation, ratcheting strain rate, strain energy density and related properties at a constant stress rate have been presented in the current study. But, the present investigation is limited at room temperature and needs further exploration. The suggested scope of future work are as follows:

1. To investigate microstructural evolution of materials at intermediate stages.
2. To study the effect of solution treatment on ratcheting properties.
3. To analyze the ratcheting characteristics at different stress rate.
4. To investigate the ratcheting behavior at different temperatures.

REFERENCES

1. Lakhtin,Y., Engineering Physical Metallurgy, Mir Publishers Moscow, 1st Edition
2. I. M. Association, "Practical guidelines for the fabrication of high performance austenitic stainless steels," ed: London, 2010.
3. S.G. Sundara Raman and K. Padmanabhan, "Tensile deformation-induced martensitic transformation in AISI 304LN austenitic stainless steel," Journal of Materials Science Letters, vol. 13, pp. 389-392, 1994.
4. P. Lambert, in Sustainability of Construction Materials (Second Edition), 2016
5. M. F. McGuire, Stainless steels for design engineers: Asm International, 2008
6. A. Sarkar, P. S. De, J. K. Mahato, A. Kundu, and P. Chakraborti, "Effect of Mean Stress and Solution Annealing Temperature on Ratcheting Behaviour of AISI 304 Stainless Steel," Procedia Engineering, vol. 74, pp. 376-383, 2014.
7. Bikram Jit Singh, “Effect of carbide precipitation on 316L stainless steel welded joints” Notion press India, 2021
8. B. Weiss and R. Stickler, "Phase instabilities during high temperature exposure of 316 austenitic stainless steel," Metallurgical transactions, vol. 3, pp. 851-866, 1972
9. M. Bayraktar, N. Tahrali, and R. Guclu, "Reliability and fatigue life evaluation of railway axles," Journal of mechanical science and technology, vol. 24, pp. 671-679, 2010.
10. G. E. Dieter and D. J. Bacon, Mechanical metallurgy vol. 3: McGraw-Hill New York, 1986.
11. J. Morrow, "Cyclic plastic strain energy and fatigue of metals," in internal friction, damping, and cyclic plasticity, ed: ASTM International, 1965.
12. A. Rohatgi, K. S. Vecchio, and I. G. T. Gray, "A metallographic and quantitative analysis of the influence of stacking fault energy on shock-hardening in Cu and Cu–Al alloys," *Acta Materialia*, vol. 49, pp. 427-438, 2001.
13. S. Asgari, E. El-Danaf, S. R. Kalidindi, and R. D. Doherty, "Strain hardening regimes and microstructural evolution during large strain compression of low stacking fault energy fcc alloys that form deformation twins," *Metallurgical and Materials Transactions A*, vol. 28, pp. 1781-1795, 1997.
14. E. El-Danaf, S. R. Kalidindi, and R. D. Doherty, "Influence of grain size and stacking-fault energy on deformation twinning in fcc metals," *Metallurgical and Materials Transactions A*, vol. 30, pp. 1223-1233, 1999.
15. U. F. Kocks and H. Mecking, "Physics and phenomenology of strain hardening: the FCC case," *Progress in Materials Science*, vol. 48, pp. 171-273, 2003.
16. E. Nes, "Modelling of work hardening and stress saturation in FCC metals," *Progress in Materials Science*, vol. 41, pp. 129-193, 1997.
17. Y. H. Zhao, Y. T. Zhu, X. Z. Liao, Z. Horita, and T. G. Langdon,"Tailoring stacking fault energy for high ductility and high strength in ultrafine grained Cu and its alloy," *Applied Physics Letters*, vol. 89, p. 121906, 2006.

18. C. Gaudin and X. Feaugas, "Cyclic creep process in AISI 316L stainless steel in terms of dislocation patterns and internal stresses," *Acta Materialia,* vol. 52, pp. 3097-3110, 2004.
19. X. Feaugas and C. Gaudin, "Ratchetting process in the stainless steel AISI 316L at 300 K: an experimental investigation," *International Journal of Plasticity,* vol. 20, pp. 643-662, 2004.
20. S. K. Paul, S. Sivaprasad, S. Dhar, and S. Tarafder, "True stress control asymmetric cyclic plastic behavior in SA333 C–Mn steel," *International Journal of Pressure Vessels and Piping,* vol. 87, pp. 440-446, 2010.
21. K. Dutta and K. K. Ray, "Ratcheting strain in interstitial free steel," *Materials Science and Engineering: A,* vol. 575, pp. 127-135, 2013.
22. S. K. Paul, S. Sivaprasad, S. Dhar, and S. Tarafder, "Ratcheting and low cycle fatigue behavior of SA333 steel and their life prediction," *Journal of Nuclear Materials,* vol. 401, pp. 17-24, 2010.
23. G. Kang, Y. Liu, and Z. Li, "Experimental study on ratchetting-fatigue interaction of SS304 stainless steel in uniaxial cyclic stressing," *Materials Science and Engineering: A,* vol. 435–436, pp. 396-404, 2006.
24. S. C. Kulkarni, Y. M. Desai, T. Kant, G. R. Reddy, Y. Parulekar, and K. K. Vaze, "Uniaxial and biaxial ratchetting study of SA333 Gr.6 steel at room temperature," *International Journal of Pressure Vessels and Piping,* vol. 80, pp. 179-185, 2003.
25. S. J. Park, K. S. Kim, and H. S. Kim, "Ratcheting behaviour and mean stress considerations in uniaxial low-cycle fatigue of Inconel 718 at 649 °C," *Fatigue & Fracture of Engineering Materials & Structures,* vol. 30, pp. 1076-1083, 2007.
26. G. Chen, X. Chen, and C.-D. Niu, "Uniaxial ratcheting behavior of 63Sn37Pb solder with loading histories and stress rates," *Materials Science and Engineering: A,* vol. 421, pp. 238-244, 2006.
27. S. K. Paul, S. Sivaprasad, S. Dhar, and S. Tarafder, "Key issues in cyclic plastic deformation: Experimentation," *Mechanics of Materials,* vol. 43, pp. 705-720, 2011.
28. C. Gupta, J. K. Chakravartty, G. R. Reddy, and S. Banerjee, "Uniaxial cyclic deformation behaviour of SA 333 Gr 6 piping steel at room temperature," *International Journal of Pressure Vessels and Piping,* vol. 82, pp. 459-469, 2005.
29. Y. Liu, G. Kang, and Y. Dong, "Experimental study on ratcheting-fatigue interaction of 20 carbon steel in uniaxial cyclic loading," 2008, pp. 73751K-73751K-5.
30. P. S. De, P. C. Chakraborti, B. Bhattacharya, M. Shome, and D. Bhattacharjee, "Ratcheting Behavior of a Titanium-Stabilized Interstitial Free Steel," *Metallurgical and Materials Transactions A,* vol. 44, pp. 2106-2120, 2013.
31. Y. Liu, G. Kang, and Q. Gao, "Stress-based fatigue failure models for uniaxial ratchetting–fatigue interaction," *International Journal of Fatigue,* vol. 30, pp. 1065-1073, 2008.
32. F. Yoshida, "Uniaxial and biaxial creep-ratcheting behavior of SUS304 stainless steel at room temperature," *International Journal of Pressure Vessels and Piping,* vol. 44, pp. 207-223, 1990/01/01 1990.

33. Kang and Y. Liu, "Uniaxial ratchetting and low-cycle fatigue failure of the steel with cyclic stabilizing or softening feature," *Materials Science and Engineering: A*, vol. 472, pp. 258-268, 2008.
34. L. Kunz and P. Lukáš, "Cyclic stress-strain behavior of 9Cr1Mo steel at positive mean stress," *Materials Science and Engineering: A,* vol. 319–321, pp. 555-558, 2001.
35. K. Dutta and K. K. Ray, "Ratcheting phenomenon and post-ratcheting tensile behaviour of an aluminum alloy," *Materials Science and Engineering: A,* vol. 540, pp. 30-37, 2012.
36. P. S. De, A. Kundu, and P. C. Chakraborti, "Effect of prestrain on tensile properties and ratcheting behaviour of Ti-stabilised interstitial free steel," *Materials & Design,* vol. 57, pp. 87-97, 2014.
37. J. Pokluda and P. Stanek, "Cyclic creep of 12010 and 14331 steels," *Kovove Mater,* vol. 16, pp. 583-599, 1978.
38. G. Kang, Y. Liu, Y. Dong, and Q. Gao, "Uniaxial Ratcheting Behaviors of Metals with Different Crystal Structures or Values of Fault Energy: Macroscopic Experiments," *Journal of Materials Science & Technology,* vol. 27, pp. 453-459, 2011/01/01 2011.
39. G. J., "Mechanics Applied to Engineering," *Longmans Green and Co.,* 1899.
40. M. J., "Cyclic plastic strain energy and fatigue of metals," *in Internal friction, damping, and cyclic plasticity,* vol. ed: ASTM International, 1965.
41. K. N. Smith, P. Watson, and T. H. Topper, "A stress-strain function for the fatigue of metals," *Journal of Materials* vol. 4, pp. 767-778, 1970.
42. S. Kwofie and H. D. Chandler, "Fatigue life prediction under conditions where cyclic creep–fatigue interaction occurs," *International Journal of Fatigue,* vol. 29, pp. 2117-2124, 2007.
43. X. Yang, "Low cycle fatigue and cyclic stress ratcheting failure behavior of carbon steel 45 under uniaxial cyclic loading," *International Journal of Fatigue,* vol. 27, pp. 1124-1132, 2005.
44. N. Miura and Y. Takahashi, "High-cycle fatigue behavior of type 316 stainless steel at 288 °C including mean stress effect," *International Journal of Fatigue,* vol. 28, pp. 1618-1625, 2006.
45. Upadhyaya, A., G. S. Upadhyaya and K.-I. Takagi, Powder Metallurgy: Science,
46. Technology and Materials. 2011: Universities Press
47. Stainless steel grade datasheets published by Atlas steels Technical Department.
48. Raj Kumar Yadav and K.P Ajit, “Recent advancement in the experimental study of ratcheting: A critical review,” vol. 2341, 020037 (2021)
49. S. Takaki, Y. Fujimura, K. Nakashima and T. Tsuchiyama, “Effect of dislocation on the yielding of highly dislocated Iron”, Materials science forum, vol. 539, pp 228-233, 2007
50. Bhaduri, A. (2018). Fracture. In: Mechanical Properties and Working of Metals and Alloys. Springer Series in Materials Science, vol 264

51. Tizziano Belleze, G. Guiliani, G. Roventi and R. Fratesi, “Corrosion behaviour of austenitic and duplex stainless steels in an industrial acidic solution,” Materials and corrosion, 16, pp. 831-838, 2016
52. Milton steels, https://miltonsteel.in/ss-316L-stainless-steel-seamless-pipe.html”
53. S. K. Paul,” A critical review of experimental aspects of in ratcheting fatigue: microstructure to specimen to component.”, JMR&T, 8(5), pp 4894-4914, 2019
54. De, A. K., Murdock, D. C., Mataya, M.C., Speer, J. G. and Matlock, D. K. (2000), Quantitative measurement of deformation-induced martensite in 304 stainless steel by X-ray diffraction, Scripta Materialia, Vol. 50, pp. 1445–1449.
55. Ulbrich Stainless Steels and Special Metal Inc. copyright ©2022.
56. J. H. Hollomon, “Tensile deformation,” Transactions of the metallurgical society of AIME, pp. 268-290, 1945
57. C. Dasarathy and T. J. Goodwin, Metals and Materials, vol. 21, 1990.